Review

Ultra-High Contrast MRI of the Brain and Spinal Cord Using Directly Acquired and Synthetic BipoLAr Inversion Recovery (BLAIR) Images

Daniel M. Cornfeld , Paul Condron , Mark Bydder , Tracy R. Melzer , Emanuele Pravatà , John D. Port , Samantha J. Holdsworth , Graeme M. Bydder *

Posted Date: 22 July 2025

doi: 10.20944/preprints202505.2380.v6

Keywords: ultra-high contrast (UHC); divided subtracted inversion recovery (dSIR) sequence; logarithmic subtracted inversion recovery (lSIR) sequence; double inversion recovery (DIR) sequence; bipolar inversion recovery (BLAIR) sequence; synthetic MRI; mild traumatic brain injury (mTBI); multiple sclerosis; whiteout sign; grayout signs

Review

Ultra-High Contrast MRI of the Brain and Spinal Cord Using Directly Acquired and Synthetic BipoLAr Inversion Recovery (BLAIR) Images

Daniel M. Cornfeld [1,2], Paul Condron [1,2], Mark Bydder [1], Tracy R. Melzer [3,4], Emanuele Pravata [5,6], John D. Port [7], Samantha J. Holdsworth [1,2] and Graeme M. Bydder [1,8,*]

[1] Matai Medical Research Institute, Tairāwhiti Gisborne, New Zealand
[2] Department of Anatomy and Medical Imaging, Faculty of Medical and Health Sciences & Centre for Brain Research, University of Auckland, New Zealand
[3] Te Kura Mahi ā-Hirikapo, School of Psychology, Speech and Hearing, University of Canterbury, Christchurch, New Zealand
[4] New Zealand Brain Research Institute, Christchurch, New Zealand
[5] Department of Neuroscience, Imaging and Clinical Sciences, Università G. d'Annunzio, via Luigi Polacchi, 66100 Chieti, Italy
[6] Neurocenter of Southern Switzerland, EOC, via Tesserete 46, 6903 Lugano, Switzerland
[7] Department of Radiology, Mayo Clinic, Rochester, Minnesota, USA
[8] Department of Radiology, University of California San Diego, San Diego, U.S.A
Correspondence: gbydder@health.ucsd.edu

Abstract

Ultra-high contrast (UHC) MRI is a term used to describe MR imaging that shows abnormalities with high contrast when little or no abnormality is seen on common conventional state-of-the-art MR images. It is achieved without the use of increased static or gradient magnetic fields. UHC can be accomplished by using tissue properties such as T_1 and T_2 twice or more in the same sequence. This synergistically contributes to overall contrast as with directly acquired divided subtracted inversion recovery (dSIR) T_1-BipoLAr Inversion Recovery (BLAIR) sequences. These sequences can also provide high contrast and high spatial resolution signal boundaries. UHC MRI can also be achieved by applying synthetic bipolar filters to high quality tissue property maps. Illustrative cases of mild traumatic brain injury, multiple sclerosis, methamphetamine substance use disorder, Parkinson's disease and white matter changes associated with a cerebral tumour are shown. Patients showed widespread abnormalities with directly acquired and synthetic dSIR and other BLAIR images in areas where little or no abnormality was seen on conventional T_2-w spin echo and/or T_2-FLAIR images. New signs seen on BLAIR images include the whiteout sign and grayout signs as well as the bilaminar cortex and bubble signs. dSIR and other BLAIR sequences create high contrast from small changes in T_1 as well as other tissue properties, and are complementary to conventional clinical sequences which create high contrast from larger changes in T_1 and/or T_2. Comparison is made with other sequences which use single or combined inversion recovery images. Four types of BLAIR sequences are described. They utilise sequences that already exist on most MR machines and are easy to implement.

Keywords: ultra-high contrast (UHC); divided subtracted inversion recovery (dSIR) sequence; logarithmic subtracted inversion recovery (lSIR) sequence; double inversion recovery (DIR) sequence; bipolar inversion recovery (BLAIR) sequence; synthetic MRI; mild traumatic brain injury (mTBI); multiple sclerosis; whiteout sign; grayout signs

 doi:10.20944/preprints202505.2380.v6

Introduction

Ultra-high contrast (UHC) MRI is a term used to describe MR imaging that shows abnormalities with high contrast when little or no abnormality is seen using common conventional state-of-the-art MRI sequences. It is achieved without the use of increased static or gradient magnetic fields. For soft tissues, Xray CT can be regarded as high contrast, conventional state-of-the-art MRI as very high contrast and MRI which shows abnormalities with obvious contrast when they are not seen with conventional MRI as UHC [1].

A common mechanism for achieving UHC MRI is synergistic contrast in which changes in a tissue property such as T_1 or T_2 are used twice or more in the same sequence to increase contrast rather than just using changes in a single property once which is the case with most conventional sequences [2]. An example is the divided subtracted inversion recovery (dSIR) sequence in which the signals from two inversion recovery (IR) sequences with different inversion times (TIs) are subtracted to increase the contrast produced by small changes in T_1. This contrast is increased further by division of the subtraction by the sum of the signals from the two sequences [3].

Another way of achieving UHC MRI is to use a high quality single tissue property map such as a T_1 or T_2 map and retrospectively apply a shaped filter to the map. The filter can increase contrast in one or more domains of tissue property values and maintain anatomical detail in the rest of the image. This is unlike narrow windowing of images which, when used to increase contrast, is accompanied by saturation of the display gray scale at the upper and lower signal thresholds. As a result, narrow windowing leads to loss of anatomical detail and limits the degree to which contrast can be increased by windowing.

The principal clinical focus of UHC MRI to date has been on small changes in tissue properties from normal. When normal and/or abnormal structures are already seen with high contrast using conventional sequences, there is no particular clinical gain in demonstrating them with even greater contrast. As a result, UHC MRI has been directed at normal or near normal appearing tissues seen with conventional state-of-the-art images where there is little or no apparent lesion contrast with the aim of demonstrating abnormalities with high contrast.

Small changes in T_1 may produce obvious abnormalities with the dSIR sequence as illustrated in a case of mild traumatic brain injury (mTBI) in an 24-year-old male patient (Figure 1). No abnormality is seen on the T_2-FLAIR image in the patient (Figure 1A). The dSIR sequence in a normal age matched control shows normal white matter in the cerebral hemispheres as low signal (dark) in Figure 1B (arrows). The same dSIR sequence in the patient shows abnormal high signal in his entire white matter (Figure 1C) (arrows). High signal (light) well defined boundaries are also seen between normal white and gray matter on the dSIR image in Figure 1B. These are less obvious in Figure 1C because of the high signal in the abnormal white matter.

High contrast abnormalities in white matter have been seen using dSIR T_1-BipoLAr Inversion Recovery (T_1-BLAIR) images of the type illustrated in Figure 1 in areas where little or no abnormality has been seen on T_2-FLAIR or T_2-wSE images in cases of mTBI [4], multiple sclerosis (MS) [5], methamphetamine substance use disorder [6] and Grinker's myelinopathy [7].

The purpose of this educational review is to describe the basic physics underlying four types of BLAIR images and illustrate their use in normal human subjects and patients.

 doi:10.20944/preprints202505.2380.v6

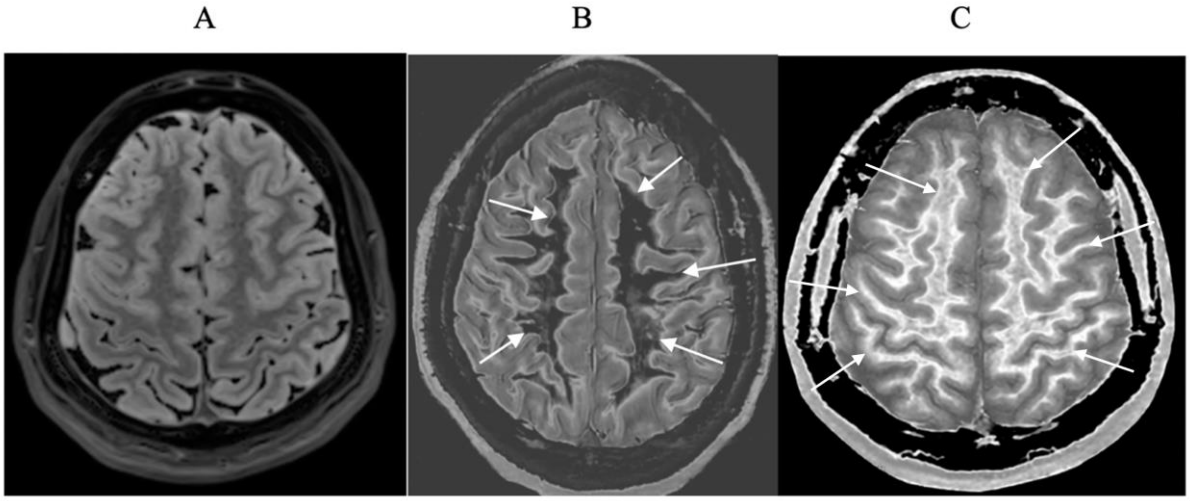

Figure 1. Positionally matched images of the brain in a 24-year-old male patient with mTBI (A and C) and a normal control (B). (A) is a T_2-FLAIR image in the patient which shows no abnormality. (B) is a narrow mD dSIR (T_1-BLAIR) image of the brain in the normal control. The white matter in the central region of this image has a normal low signal (dark) appearance (arrows). (C) is a narrow mD dSIR (T_1-BLAIR) image performed in the patient with the same sequence as in the control. This image shows all the patient's white matter with abnormal high signal (light) (arrows) rather than the normal low signal (dark) appearance in the control (arrows) (B). There is a night and day difference in signal between normal and abnormal white matter in (B) and (C). High signal boundaries are seen between normal white matter and normal gray matter in (B). These are less obvious in (C) because of the high signal in the abnormal white matter.

Basic Physics

Tissue Property Filters (TP-filters) and the Inversion Recovery (IR) Sequence

The first part of this paper is a condensed and updated version of work published previously [1-3]. It is included to make the paper self-contained and not require concurrent reference to other papers to understand the contrast seen on BLAIR images included in this paper.

Instead of illustrating image contrast in the usual way by plotting longitudinal and then transverse magnetisation (M_Z and then M_{XY}) against time using the Bloch equations as in Figure 2, it is possible to use plots of signals produced by the exponential recovery of longitudinal magnetisation and exponential decay of transverse magnetisation against T_1 and T_2 respectively (rather than against time). These plots are tissue property-filters (TP-filters); the tissue properties may be mobile proton density (ρ_m), T_1, T_2, T_2*, D*, etc [8, 9]. (In this paper the term tissue is used to include fluids unless otherwise specified.)

For TR >> T_1, the T_1 dependent part of the IR sequence has the signal equation:

$$S_{T1} = 1\text{-}2e^{-TI/T_1} \qquad (1)$$

where S_{T1} is the signal from the T_1-filter, TI in the inversion time and T_1 is the longitudinal relaxation time. The T_1-filter of the IR sequence (with a constant value of TI) is shown in phase-sensitive or signed form in Figure 3A where it is a monotonic low pass filter, and in magnitude form in Figure 3B where it is a negative unipolar T_1-filter. The maximum size of the slopes of these two filters are shown with red lines in Figs. 3A and 3B. The magnitude forms of the IR filter $S_{T1} = (1\text{-}2e^{-TI/T_1})$ for $T_1 < \frac{TI}{\ln 2}$ and $S_{T1} = (2e^{-TI/T_1} - 1)$ for $T_1 > \frac{TI}{\ln 2}$ are used in the subsequent text unless otherwise specified.

 doi:10.20944/preprints202505.2380.v6

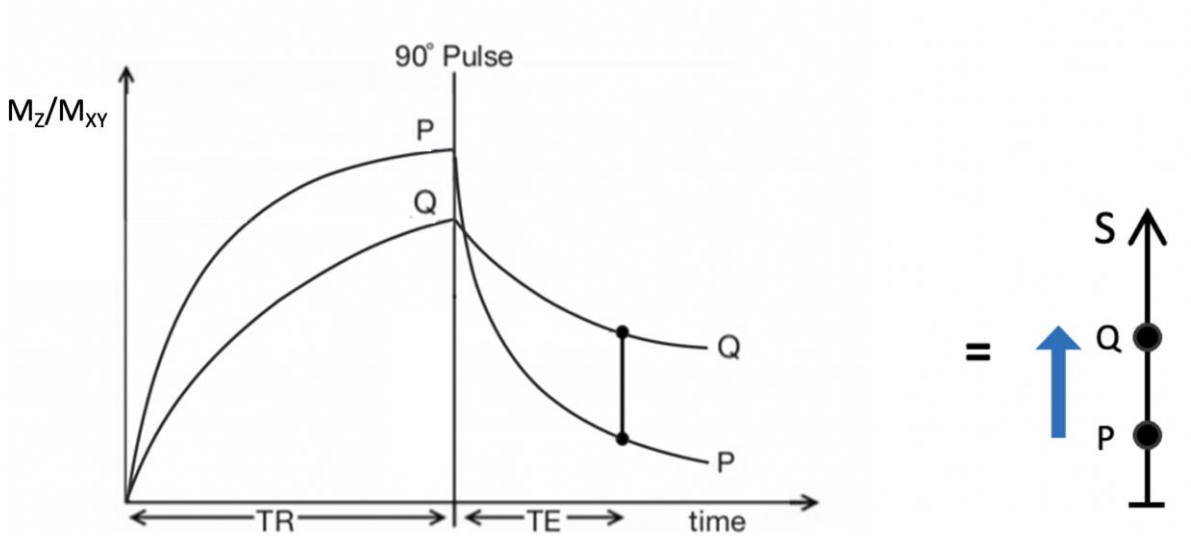

Figure 2. Plot of M_Z/M_{XY} against time for a T_2-weighted version of the SE sequence for two tissues P (with a shorter T_1 and T_2) and Q (with a longer T_1 and T_2). Overall T_1 and T_2 dependent contrast between P and Q is shown with the positive blue arrow on the right.

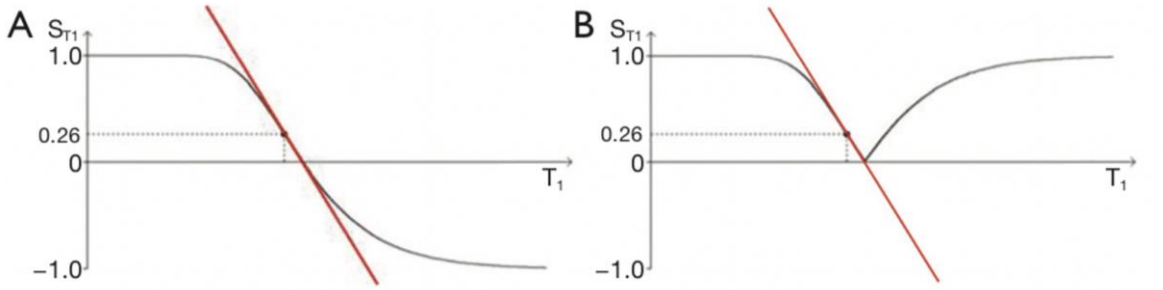

Figure 3. IR T_1-filters with plots of signal S_{T1} against T_1 in phase-sensitive (A) and magnitude forms (B). (A) is a low pass filter and (B) is a negative unipolar filter. (A) shows both positive and negative values for S_{T1} whereas (B) shows negative values "reflected" across the X axis so they become positive. The maximum size of the slopes of the two T_1-filters which are tangential to the slope are shown as red lines. The slopes are negative in both cases. .

When TI is increased, the magnitude IR unipolar T_1-filter shifts to the right as shown in Figure 4. Figure 4A (left) shows the IR T_1-filter with a short TI_s (e.g., the Short TI IR or STIR sequence) for brain where gray matter (G) has a higher signal than white matter (W). The slope of the T_1-filter between W and G is moderately positive (red line).

When the TI is increased to an intermediate TI, TI_i, as in Figure 4B (centre), the T_1-filter is shifted to the right. W and G are fixed in the same position on the X axis, and W now has a higher signal than G. The slope of the T_1-filter between W and G is strongly negative (red line).

When the TI is increased further to a long TI, TI_l, the T_1-filter is displaced further to the right, as in Figure 4C (right) where W has a slightly higher signal than G, and the slope of the T_1-filter between them is mildly negative (red line).

Using the small change approximation of differential calculus, the contrast (difference in signal) produced by each T_1-filter from the increase in T_1 from W to G (horizontal green arrows in Figs. 4A, 4B and 4C) is the size of this increase multiplied by the slopes of the respective T_1-filters (i.e. by their first derivatives, the red lines). This contrast is shown by the vertical blue arrows in Figure 4 and is

 doi:10.20944/preprints202505.2380.v6

moderately positive in Figure 4A, highly negative in Figure 4B and mildly negative in Figure 4C. In each example, the slopes of the T_1-filters show the contribution of the sequence to contrast.

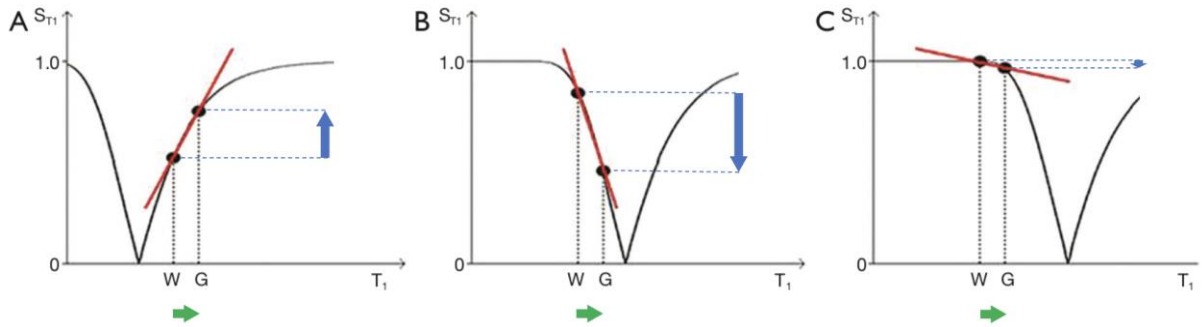

Figure 4. The long TR IR sequence. Negative unipolar T_1-filters for short TI_s (A, left), intermediate TI_i (B, centre) and long TI_l (C, right) including white (W) and gray (G) matter. Signal S_{T1} is plotted against T_1 in each case (black curves). The positions of W and G are the same at each of the three TIs. TI is increased from TI_s (left) to TI_i (centre) and increased further to TI_l (right). In (A), (B) and (C), the increase in T_1 from W to G (horizontal positive green arrows) is multiplied by the relevant slopes of the filters (red lines) to produce contrast. This is moderately positive, strongly negative, and mildly negative contrast in (A), (B) and (C) respectively (vertical blue arrows).

Subtracted IR (SIR) and divided Subtracted IR (dSIR) Bipolar Filters

Two conventional magnitude IR negative unipolar T_1-filters with different TIs, namely TI_{short} = TI_s and $TI_{intermediate}$ = TI_i are shown in Figure 5A. The subtraction: first TI_s T_1-filter minus the second TI_i T_1-filter produces the subtracted IR (SIR) bipolar T_1-filter shown in Figure 5B. The vertical dashed lines at the null points of the two IR T_1-filters shown in Figure 5A divide the X axis in Figure 5B into the lowest Domain (lD), the middle Domain (mD) and the highest Domain (hD). In the mD in Figure 5B (between the two dashed lines) the size of the slope of the SIR bipolar T_1-filter is about double that of the IR T_1-filters shown in Figure 5A. This is because the slope of the SIR filter in its mD in Figure 5B is the positive slope of the TI_s filter in the mD shown in Figure 5A minus the negative slope of the TI_i filter in the mD also shown in Figure 5A.

The two IR T_1-filters shown in Figure 5A can also be added to give the Added IR (AIR) T_1-filter shown in Figure 5C. In its mD, which is bounded by the vertical dashed lines, the signal is reduced to about 0.20 compared with its value of 2 at $T_1 = 0$ (i.e. about one tenth).

Figure 6A shows a divided SIR (dSIR) bipolar T_1-filter in which the SIR bipolar T_1-filter in Figure 5B is divided by the AIR T_1-filter in Figure 5C i.e. $\frac{\text{difference}}{\text{sum}}$. The signal ($S_{dSIR}$) of the dSIR filter is given by:

$$S_{dSIR} = \frac{S_{TIs} - S_{TIi}}{S_{TIs} + S_{TIi}} \qquad (2)$$

where S_{TIs} is the signal from the shorter TI filter and S_{TIi} is the signal from the intermediate TI_i filter.

 doi:10.20944/preprints202505.2380.v6

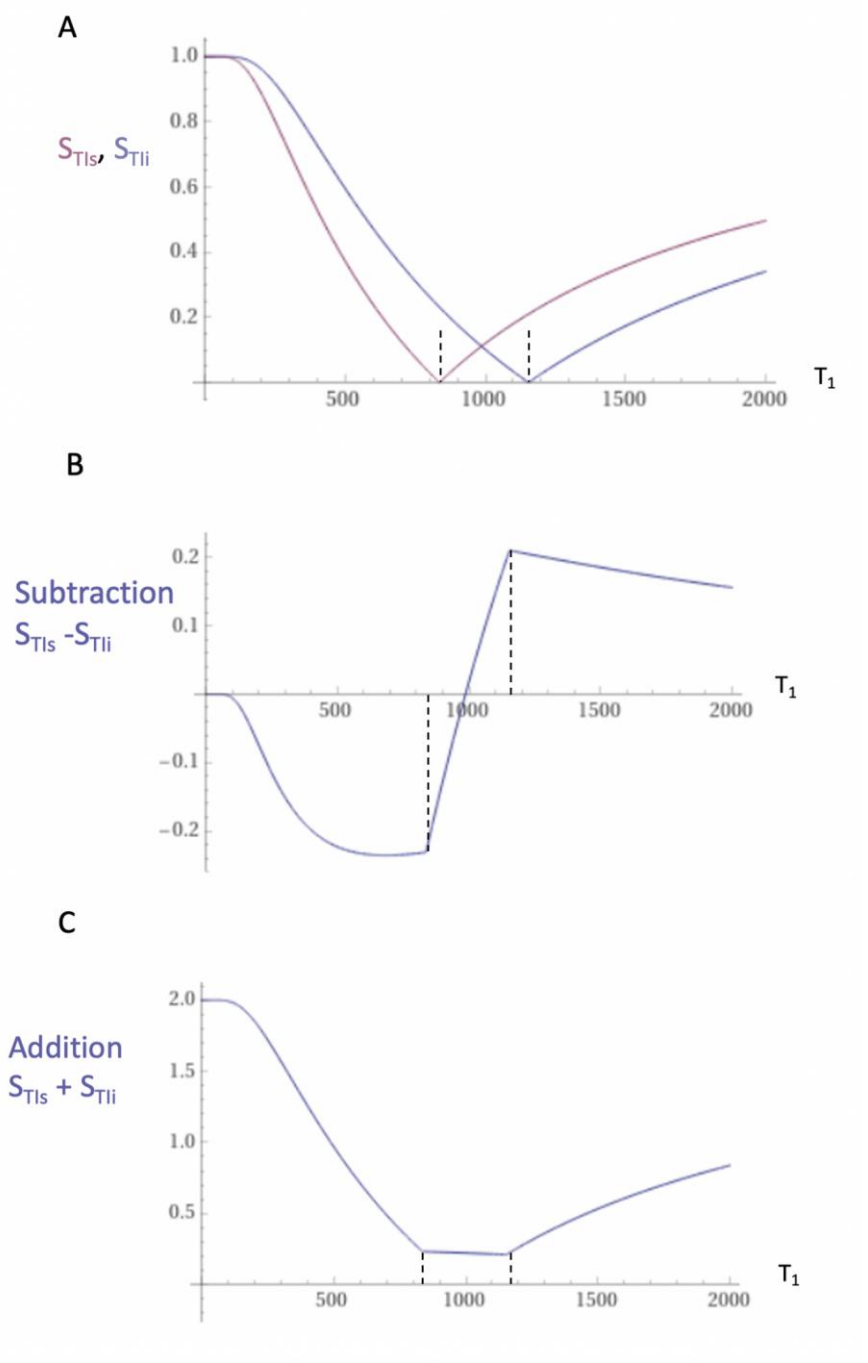

Figure 5. Unipolar IR (A), subtracted IR (SIR) (B) and Added IR (AIR) (C) T_1-filters. T_1 is shown along the X axes in ms. (A) shows a TI_s unipolar T_1-filter (pink) and a TI_i unipolar T_1-filter (blue), (B) shows the subtraction (S_{TIs} - S_{TIi}) IR or SIR bipolar T_1-filter, and (C) shows the addition (S_{TIs} + S_{TIi}) IR or AIR T_1- filter. The vertical lines divide the X axes into lowest, middle and highest Domains (lD, mD and hD). The mD contains T_1 values between the vertical dashed lines. In (B) the slope of the curve of the SIR T_1-filter in the mD is about double that of the S_{TIs} T_1-filter (pink in [A]). In (C) the signal at T_1=0 is doubled to 2.0, and the signal in the mD is reduced to about 0.20 in the nearly linear, slightly downward sloping central part of the AIR T_1-filter (i.e., in the mD).

The resulting dSIR bipolar T_1-filter (Figure 6A) shows a negative pole and a positive pole. Its mD shows a highly positive nearly linear slope which is about ten times greater than the slopes of the IR T_1-filters shown in Figure 5A. The dSIR filter has maximum and minimum values of ±1. The contributions from ρ_m and T_2 in conventional IR sequences cancel out with dSIR sequences which are

 doi:10.20944/preprints202505.2380.v6

therefore T_1 maps. As a result, the whole sequence can be accurately represented by its bipolar T_1-filters.

Figure 6B compares the contrast produced by a conventional S_{TIs} IR unipolar T_1-filter (pink) to that from the SIR bipolar T_1-filter (blue) shown in Figure 5B from the same increase in T_1 (horizontal positive green arrow, ΔT_1). ΔT_1 is multiplied by the slopes of the respective S_{TI} IR and SIR filters (red lines) to produce the differences in signal ΔS, i.e. the contrast from each of them. These are shown by the vertical pink and blue arrows on the right. The SIR bipolar T_1-filter generates about twice the contrast (blue arrow) of the S_{TIs} IR unipolar T_1-filter (pink arrow) from the same increase in T_1, ΔT_1.

Figure 6C compares the contrast produced by the S_{TIs} unipolar IR T_1-filter (pink) to that produced by the dSIR bipolar T_1-filter shown in Figure 6A (blue). The increase in T_1 (horizontal positive green arrow, ΔT_1) is multiplied by the slopes of the respective S_{TIs} IR and dSIR filters (red lines) to produce the differences in signal ΔS, or contrast generated by the two filters. These are shown by the vertical pink and blue arrows on the right. For the same increase in T_1 (ΔT_1), the dSIR bipolar T_1-filter produces about ten times greater contrast than the S_{TIs} IR unipolar T_1-filter. The S_{TIs} IR T_1-filter is that of a conventional TI IR sequence such as MP-RAGE (magnetisation prepared-rapid acquisition gradient echo).

 doi:10.20944/preprints202505.2380.v6

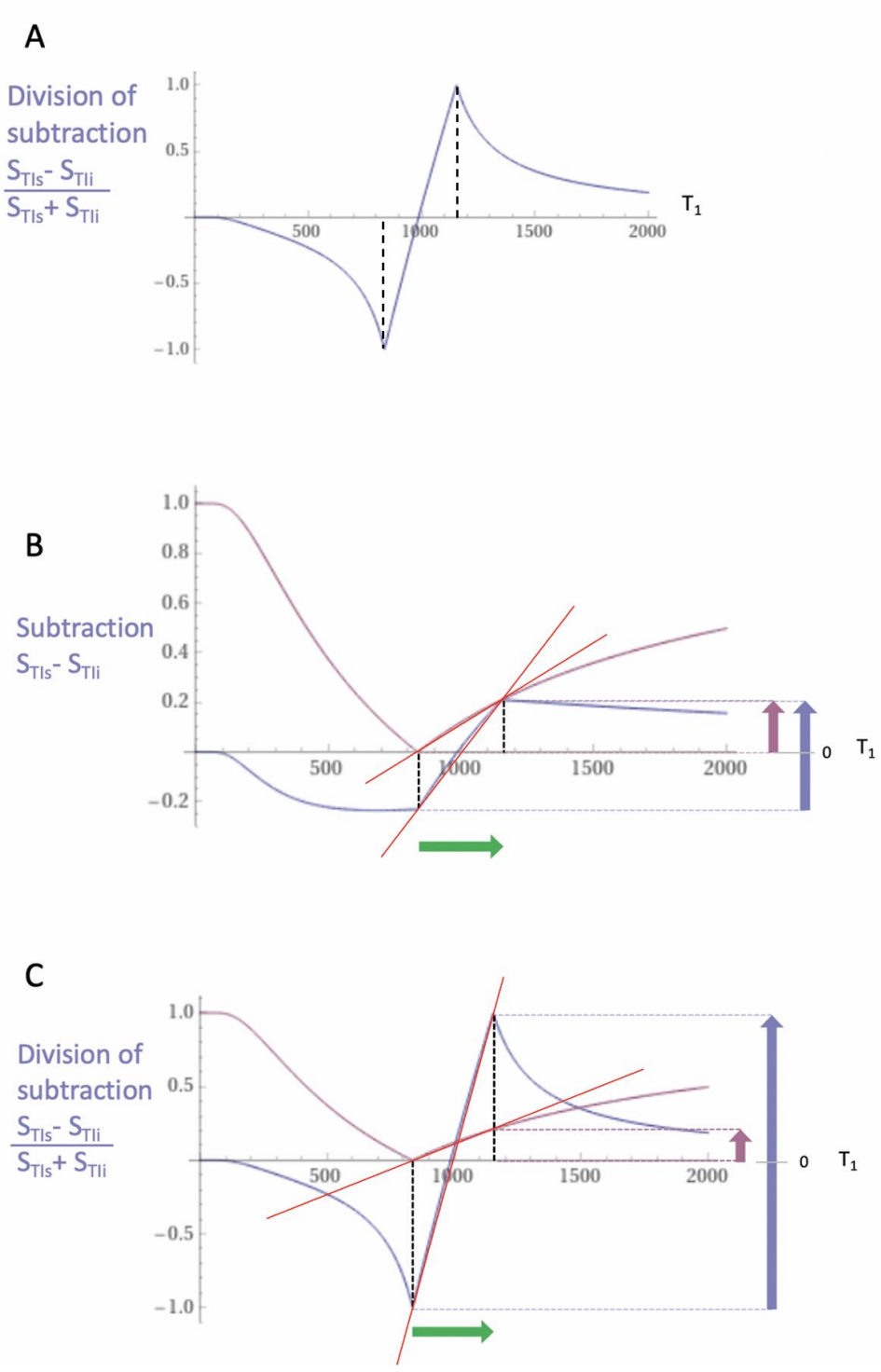

Figure 6. Fig. 6A shows division of the SIR bipolar T_1-filter in Fig. 5B by the addition T_1-filter AIR in Fig. 5C to give the dSIR bipolar T_1-filter. T_1 is shown along the X axis in ms. Fig. 6B shows comparison of the conventional IR S_{TIs} unipolar T_1-filter (pink) with the SIR bipolar T_1-filter (blue) for a small increase in T_1 (horizontal positive green arrow, ΔT_1). Fig. 6C is a comparison of the S_{TIs} unipolar T_1-filter (pink) with the dSIR bipolar T_1-filter (blue) for the same small increase in T_1. In 6B the contrast produced by the SIR bipolar T_1-filter is about twice that produced by the IR unipolar T_1-filter (blue and pink arrows). In 6C the contrast produced by the dSIR bipolar T_1-filter is about ten times greater than that produced by the IR unipolar T_1-filter (blue and pink arrows). The display gray scale has no negative values so white matter appears on it as zero signal (black) at the lowest part of the display scale when using both the T_1-filters shown in each of 6B and 6C.

 doi:10.20944/preprints202505.2380.v6

To produce the large increase in contrast shown in Figure 6C, the dSIR sequence is typically targeted at the small increase in the T_1 of normal tissue produced by disease (shown by the horizontal green arrow) and this is positioned within the steeply sloping mD of the dSIR bipolar T_1-filter. This is done by choosing appropriate values of TI_s and TI_i. The target is often small increases in the T_1 of white matter. High contrast can also be produced by difference or change in T_1 within the lower part of the hD and the upper part of the lD where the dSIR bipolar T_1-filter has relatively steep slopes. More detail is available in reference [3].

Contrast at Tissue Boundaries

MRI tissue boundaries take different forms such as a gradual change in signal from one tissue to another as well as sharply defined high and low signal boundaries between tissues. In the boundary region between two pure tissues (such as between white and gray matter) the T_1s of voxels which contain mixtures of the two tissues typically span the range of T_1 values between those of the two pure tissues. If a narrow mD dSIR bipolar T_1-filter (e.g., with TI_s nulling normal white matter, and TI_i longer than TI_s but less than that needed to null gray matter) is used there are mixtures of white and gray matter in voxels in the boundary region between the two tissues which have intermediate T_1 values ($T_{1W,G}$) that correspond with the peak of the bipolar T_1-filter as shown in Figure 7. This produces a high signal boundary between white matter and gray matter. The dSIR bipolar T_1-filter shows much higher contrast than that produced between white matter and gray matter by a conventional white matter nulled IR sequence such as MP-RAGE (Figure 7). The mechanism shown in Figure 7 produces the high signal $S_{W,G}$ at the boundary between normal white and normal gray matter shown in Figure 1B. High signal boundaries are also seen at the junction between CSF and white matter at ventricular boundaries, and can be seen at the boundary between gray matter and CSF with wide mD sequences [3].

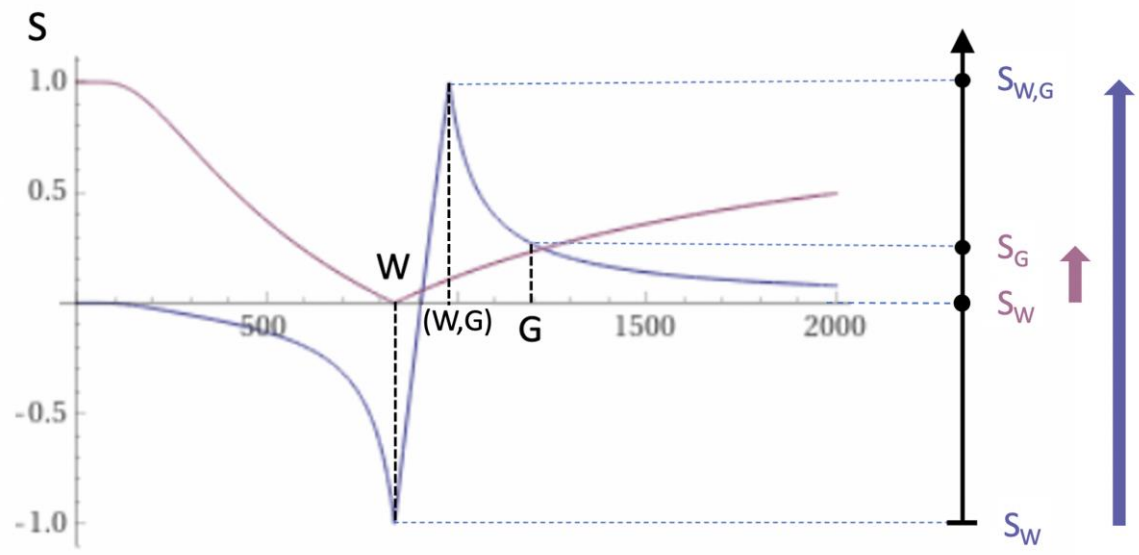

Figure 7. Boundaries. This image shows a narrow mD dSIR bipolar T_1-filter with a mD extending from white matter (W) to a $T_{1W,G}$ between the TIs of W and gray matter (G) (blue curve) as well as a white matter nulled conventional IR unipolar T_1-filter e.g., MP-RAGE (pink curve). The X axis is shown in ms. The contrast produced from the difference in signal between W and G by the unipolar T_1-filter is (S_G minus S_W, pink curve) and is shown by the vertical pink arrow. With the bipolar T_1-filter (blue curve) there is a partial volume effect between W and G producing a $T_{1W,G}$ between the T_1s of W and G which results in the high signal, $S_{W,G}$ shown on the bipolar T_1-filter (blue curve). The contrast between this high signal and white matter is the difference ($S_{W,G}$ minus S_W, in blue) and is shown by the vertical blue arrow. The contrast produced by the bipolar T_1-filter at the boundary between W and G is far greater than that produced at the boundary between W and G by the unipolar T_1-filter.

 doi:10.20944/preprints202505.2380.v6

T_1 Maps and Qualitative - Quantitative MRI

To better understand the dSIR bipolar T_1-filter, a linear equation of the form y = mx + c can be used to approximate the filter in its mD. The equation is produced by fitting a straight line between the first and last points of the mD (i.e. first point x = $\frac{TI_s}{\ln 2}$ and y = -1, and last point x = $\frac{TI_i}{\ln 2}$ and y = +1). In the mD, the signal of the dSIR sequence S_{dSIR}, is given by:

$$S_{dSIR} \approx \frac{\ln 4}{\Delta TI} T_1 - \frac{\Sigma TI}{\Delta TI} \qquad (3)$$

where $\Delta TI = TI_i - TI_s$ (i.e., second TI minus first TI) which is positive, and $\Sigma TI = TI_s + TI_i$ which is also positive. Note that because ΔTI is positive, the slope $\frac{\ln 4}{\Delta TI}$ is positive. The offset is negative.

The expression in Eq. (2) illustrates four key features of the dSIR bipolar T_1-filter, firstly, the near linear change in signal (i.e. S_{dSIR}) with T_1 in the mD, secondly, the filter has a slope in the mD equal to $\frac{\ln 4}{\Delta TI}$, thirdly the filter shows high sensitivity to small changes in T_1 when the size of ΔTI is small. When ΔT_1 is small, the size of ΔTI can be decreased to match it and so scale up the sensitivity of the filter. The reduction in ΔTI increases the steepness of the T_1-filter in the mD and thus the amplification of contrast produced from ΔT_1. This compensates for the small value of ΔT_1 until the sequence becomes SNR and/or artefact limited. This is not the case with conventional IR sequences where, if ΔT_1 is decreased, contrast decreases.

Fourthly, Eq. (3) can be used to calculate T_1 values in the mD so that:

$$T_1 \approx \frac{\Delta TI}{\ln 4} S_{dSIR} + \frac{\Sigma TI}{\ln 4} \qquad (4)$$

The linear approximation is only valid in the mD. Also, it is assumed that TR is long compared to tissue T_1 values. An equivalent expression that allows for incomplete recovery of longitudinal magnetisation during TR can be formulated.

Outside of the mD in the lD and hD, the magnitude of the dSIR bipolar T_1-filter signal decreases towards zero at minimum and maximum values of T_1. T_1s in the mD occupy the full range of the display gray scale from black to white. T_1s from the shortest and longest T_1s in the lD and hD respectively only occupy parts of the display gray scale.

Magnetisation transfer (MT) (see later) may have a substantial effect on T_1 values which can be regarded as observed T_1s reflecting the process of signal acquisition as well as T_1 as an intrinsic property of tissue.

Log Then Subtracted Inversion Recovery (lSIR) Sequences

Another bipolar T_1-filter is the natural logarithm (ln) then subtracted inversion recovery (lSIR) filter [10]. The signal of this filter (S_{lSIR}) is half of the subtraction: ln short S_{TIs} T_1-filter minus ln intermediate S_{TIi} T_1-filter. The ln S_{TIs} and ln S_{TIi} negative unipolar T_1-filters are shown in Figure 8 and have sharper negative poles than those of unipolar S_{TIs} and S_{TIi} T_1-filters shown in Figure 5A.

Figure 9 shows a dSIR bipolar T_1-filter in blue and the corresponding lSIR bipolar T_1-filter with the same TIs in orange. The two filters appear similar in the lowest region of the lD and in the highest region of the hD as well as in the central region of the mD. The slope of the dSIR filter is essentially constant and equal to $\frac{\ln 4}{\Delta TI}$. The magnitude of the slope of the lSIR filter is the same that of the dSIR filter at the centre of the mD but greater around the lower and higher nulling TI values. The lSIR filter asymptotically approaches negative and positive infinity at the two corresponding T_1s. The lSIR filter increases its contrast amplification as the change in T_1 from normal becomes smaller. Like the dSIR filter, the lSIR filter essentially eliminates the ρ_m and T_2 dependence of the full IR sequence and so can be used to model the full behaviour of the sequence.

 doi:10.20944/preprints202505.2380.v6

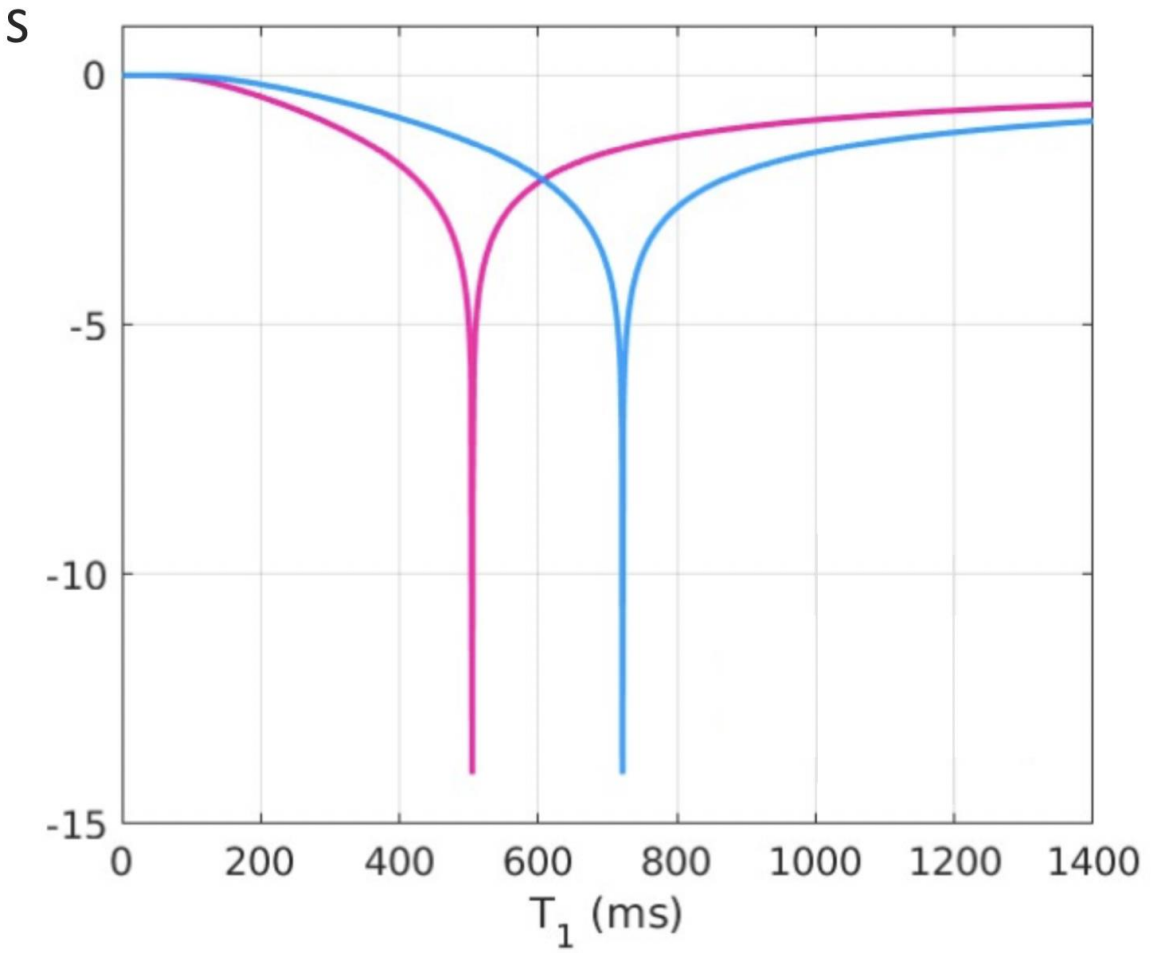

Figure 8. Plots of ln S_{TIs} (TI_s = 350 ms) vs T_1 (pink), and ln S_{TIi} (TI_i = 500 ms) vs T_1 (blue). The plots have a negative unipolar form with steeply sloping signal gradients around their negative poles. The pink and blue ln S_{TIs} and ln S_{TIi} curves are steeper than the corresponding magnitude curves shown in Fig. 5A for conventional IR T_1-filters. The lSIR filter S_{lSIR} = ½(ln S_{TIs} - ln S_{TIi}) reverses the sign of the S_{TIi} filter so it becomes positive as seen in the following figure (Fig. 9) (orange curve).

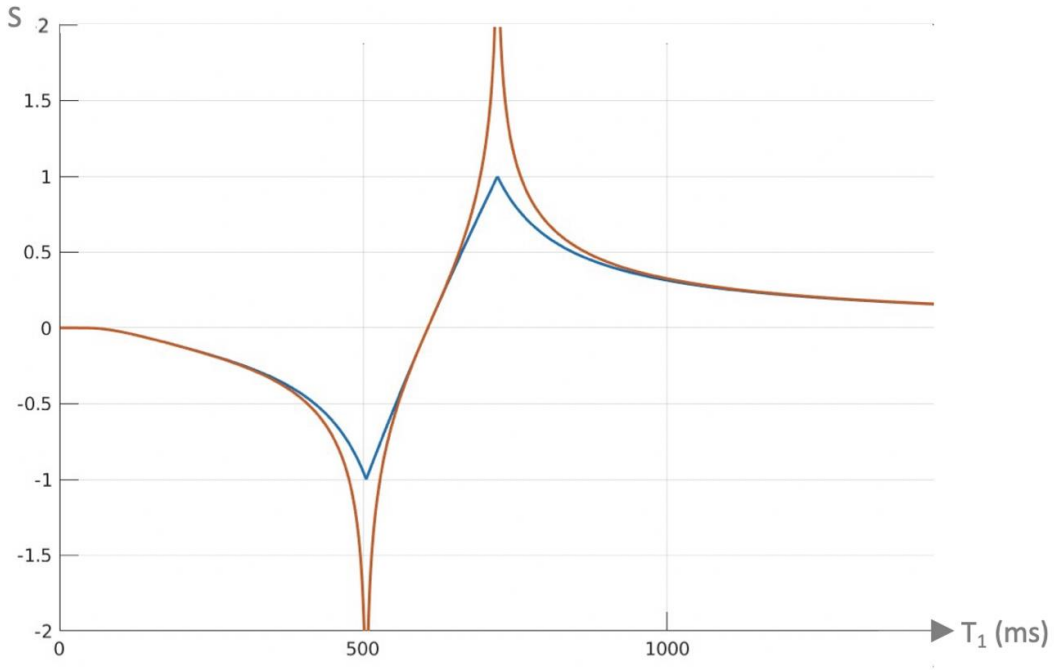

 doi:10.20944/preprints202505.2380.v6

Figure 9. Plot of signal vs T_1 in ms for a dSIR bipolar T_1-filter (blue curve) and the corresponding lSIR bipolar T_1-filter with the same null points (orange curve) (TI_s = 350 ms and TI_i = 500 ms, ΔTI = 150 ms). The dSIR filter shows the usual pattern with maximum values of ±1. It has an essentially constant slope in the mD. The lSIR filter has similar values to the dSIR filter in the regions of lowest and highest values of T_1 as well as in the centre of the mD. However around the lower and upper T_1 nulling values it has much steeper slopes and proceeds asymptotically to minus and plus infinity respectively (values of S along the Y axis in the range of ± 2 are shown). From a practical point of view, the contrast for very small differences or changes in T_1 is 2-3 times greater with the lSIR filter compared with the corresponding dSIR filter. For the same difference in T_1 in the regions close to the null points the lSIR filter is steeper than the dSIR filter. This results in greater contrast and spatial resolution.

The lSIR filter is an inverse hyperbolic tangent of the dSIR filter in the mD (S_{lSIR} = atanh S_{dSIR}), and an inverse hyperbolic cotangent of the dSIR filter in the lD and hD.

From a practical point of view, the lSIR T_1-filter has 2-3 times the slope of the dSIR T_1-filter for very small differences or changes in T_1 around the null points and thus has 20-30 times greater contrast than conventional IR sequences for the same very small differences or changes in T_1. The maximum and minimum values of the lSIR T_1-filter are usually shown as ±2-3 (rather than ±infinity). This compares with values of ±1 for the dSIR T_1-filter. The low and high signal boundaries of the lSIR T_1-filter are narrower than those of the corresponding dSIR filter. The lSIR T_1-filter shows a selective increase in slope, or sharpening, close to the nullpoints.

Composite (c) Bipolar Filters (T_1 as well as T_2, T_2*, D*, χ and/or MT)

It is possible to introduce an attenuation filter S_{OF} (other filter) and apply it to one of the two IR filters used for dSIR bipolar T_1-filter imaging in Figs. 5 and 6. S_{OF} may equal $e^{-\Delta TE/T2}$, $e^{-\Delta TE/T2^*}$ or $e^{-\Delta bD^*}$ which introduce T_2, T_2* and D* dependence respectively. This provides additional contrast to the T_1 contrast of the dSIR bipolar T_1-filter. When ΔTE equals zero, or Δb equals zero, S_{OF} = 1. If S_{OF} is set to 0.5 and 0.25, the curves shown in Figs. 10A and 10B result when using a narrow mD dSIR sequence (TIs = 350 ms and 500 ms). The nulling times are the same for all values of S_{OF}.

In Figure 10A attenuation of the first IR filter (with TI_s) is shown with S_{OF} set at 1 (blue), 0.5 (orange) and 0.25 (yellow). The yellow and orange curves are wider around the outside of the first (negative) pole at the first TI_s and are narrower and inside the second (positive) pole at TI_i. This results in a broadening and loss of contrast and lower signal white matter around the first negative pole as well as increased contrast and narrower boundaries between white and gray matter around the positive pole. S_{OF} can be set negative values to reverse the sign of the relevant contrast and make it synergistic with the T_1 contrast.

In Figure 10B, attenuation of the second IR filter (with TI_i) is shown. As S_{OF} is decreased from 1.0 to 0.5 and 0.25, the filter narrows around the first (negative) pole and widens around the second (positive) pole. The negative contrast produced for the same difference in T_1 is increased around the first negative pole. Composite (c) forms of the dSIR and lSIR bipolar T_1-filters can be designated as cdSIR, clSIR etc.

 doi:10.20944/preprints202505.2380.v6

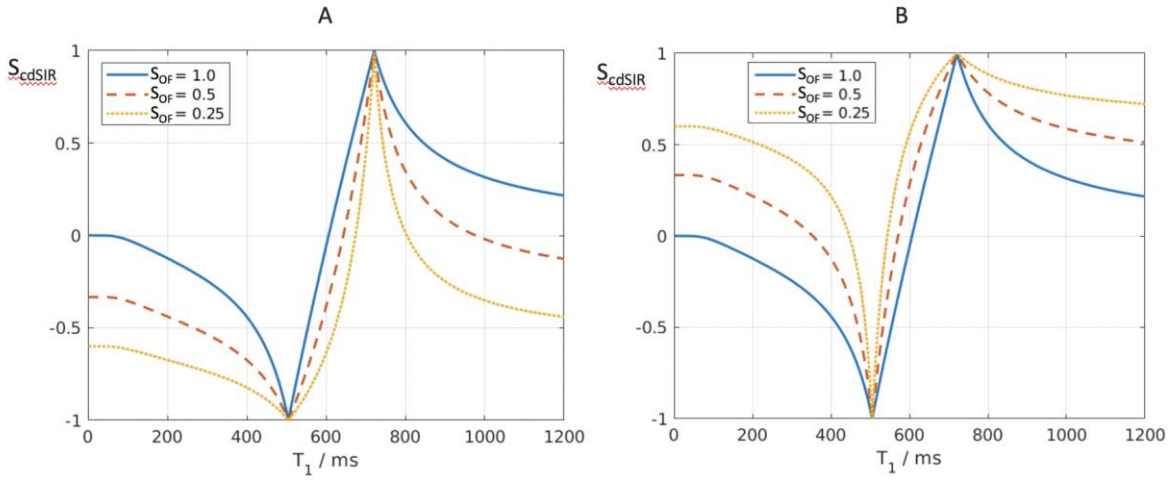

Figure 10. Composite dSIR filters (cdSIRs with TI_s = 350 ms and TI_i = 500 ms). Attenuated first IR T_1-filter (TI_s) in (A) and attenuated second IR T_1-filter (TI_i) in (B). (A) shows the conventional bipolar T_1-filter (blue) with S_{OF} = 1, an attenuated first TI_s filter (S_{OF} = 0.5) (red) and a further attenuated first TI_s filter (S_{OF} = 0.25) (yellow). In (A), as S_{OF} is decreased to 0.5 and 0.25 the filters around the first negative pole become wider and are positioned outside the blue filter. The attenuated filters around the second positive pole show higher contrast and become narrower. They are located inside the blue filter. (B) shows the conventional bipolar T_1-filter (blue) with S_{OF} = 1, and attenuated second TI_i filter S_{OF} = 0.5 (red) and a more attenuated second TI_s filter (S_{OF} = 0.25) (yellow). As S_{OF} is decreased, the filters around the first negative pole become narrower and show higher contrast. They are positioned within the blue filter. The attenuated filters around the second positive pole become wider and show lower contrast. They are positioned outside of the blue filter. For T_2, a short T_2 increases attenuation relative to a longer T_2 and this corresponds to the narrower and sharper peak with greater negative contrast and spatial resolution of the contrast (A).

Susceptibility and MT can also be used to attenuate signals and produce supplementary contrast. The combination of T_1 and T_2* contrast may be of value in demonstrating the central vein sign and paramagnetic rim sign in multiple sclerosis (MS) as well as late sequelae of haemorrhage and fMRI in combination with perfusion.

Synthetic dSIR and lSIR Bipolar T_1-filter Images

Synthesizing narrower mD images from wider mD dSIR and lSIR bipolar T_1-filter images

It is possible to synthetically create narrower mD dSIR images from wider mD dSIR images using Eq. 1 and the relationships illustrated in Figure 6A. The TIs of the narrower mD images are within those of the wider mD when using magnitude forms of the IR sequences. MT effects may need to be included.

Synthesizing dSIR and lSIR bipolar T_1-filter images from T_1 maps

dSIR and lSIR bipolar T_1-filter images with particular values of TI can also be synthesised from T_1 maps using Eq.1 and the relationships shown in Figs. 6A, 8 and 9. T_1 and other tissue property maps (T_2, T_2*, D*) have linear TP-filters with maximum signal values at the high end of the tissue property X axis. As a result, CSF has high signals on the maps and this can dominate their appearance. The problem can be avoided when appropriate bipolar T_1-filters are applied to T_1 maps to create bipolar T_1 images in which CSF signal is reduced. The equivalent mapping using MP2RAGE acquisitions has also been described previously. While in principle the same contrast is obtained, there are wide discrepancies in the T_1s measured by different techniques suggesting T_1 is not independent of the method of acquisition with MT a major contributor to the variance. The variance may mask small white matter abnormalities seen with general purpose T_1 mapping.

 doi:10.20944/preprints202505.2380.v6

Synthesizing T_2-, T_2-, D*and χ-bipolar filter images using purpose designed bipolar filters together with T_2, T_2*, D* and χ maps*

It is also possible to create bipolar TP-filter images from tissue properties other than T_1 using purpose designed synthetic bipolar TP-filters. These filters are typically based on the appearance of the dSIR bipolar T_1-filter shown in Figs. 6A and 6C. They can have a linear function in their mD and a scaled reciprocal function (e.g., $y = \frac{a}{x}$) or similar function in their hDs and lDs. These functions join the linear function in the mD at signal values of -1 and +1, respectively. Synthetic bipolar TP-filters can then be used with T_2, T_2*, D* and χ maps to create bipolar T_2-, T_2*-, D*-and χ-filter images.

The lSIR inverse hyperbolic tangent and cotangent functions can also be used in the same way to create synthetic lSIR bipolar TP-filter images from tissue property maps.

Directly acquired bipolar T_1-filter images and synthetic bipolar T_1-, T_2-, T_2*-, D*-, and χ- images with different TPs can be multiplied together to produce synergistic bipolar multi TP-filter images. The signs of the slopes of the bipolar TP-filters (negative or positive) can be matched with the signs of the changes in tissue properties (negative or positive) to ensure the contrast produced by the different tissue properties is synergistic [2].

Window Levels and Widths of Displayed Images

Conventional Changes In Window Level and Width of MR Images

When an image is displayed, the window level sets the brightness (signal level) and the window width sets the contrast (signal difference). Changes in the window level and width of images change their signals on the gray scale display from S to S_D and can be described using a high pass filter as seen in Figure 11A. This plots the display signal S_D against the image signal S. This is a signal (S) filter not a TP-filter. Contrast (the difference in signal between the S_Ds of P and Q) may be increased by narrowing the window width as shown in Figure 11B so that P and Q are now respectively shown at the lower and upper ends of the display scale. With narrow windowing, signals with values at the upper end of the X axis from Q and beyond are all shown with the same high value of S_D. As a result, there is no contrast between these voxels and they coalesce into blocks. This leads to a loss of anatomical coherence. The same also happens at the lower end of the S scale where values of S less than P have the same signal in Figure 11B and coalesce. This saturation of signals establishes a practical limit to how tightly images can usefully be windowed (i.e., how narrow the window width can usefully be made) and thus how much the contrast of the displayed image can be increased before the loss of anatomical coherence leads to a lack of credibility of the images. This is in addition to limits imposed by SNR considerations and image artefact levels.

dSIR Images

dSIR images can decrease ΔTI and so increase contrast. Maximum and minimum values are shown as high and low signal boundaries as in Figure 11C, T_1 values lower than the lower nulling T_1 value and greater than the greater nulling T_1 value do not appear on the same plateaux as with conventional narrow windowing in Figure 11B, but vary in signal because of the sloping regions in the lDs and hDs of the dSIR bipolar T_1-filter (Figure 11C). Consequently, contrast is maintained and anatomical detail is preserved in all three Domains when ΔTI is decreased. As a result, contrast can be increased by decreasing ΔTI until it becomes SNR and/or artefact limited.

 doi:10.20944/preprints202505.2380.v6

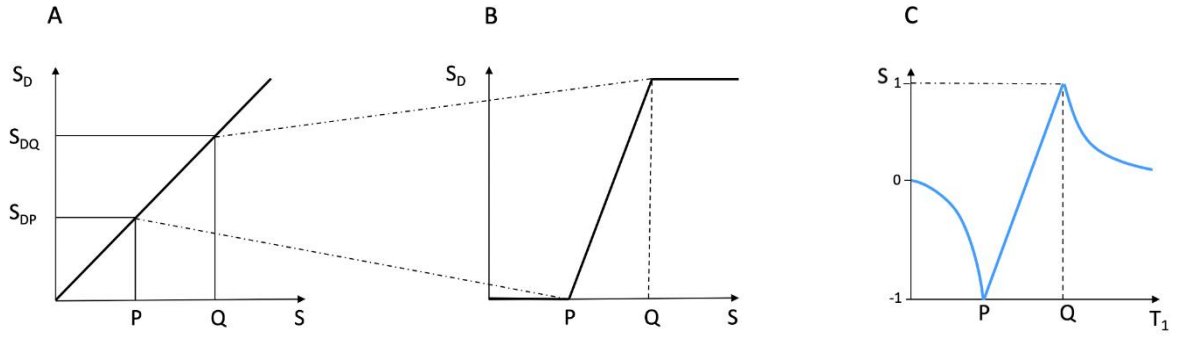

Figure 11. Comparison of conventional windowing (A and B) and a dSIR bipolar T_1-filter (C). (A) plots the display signal S_D against image signal S for two tissues P and Q over the full image gray scale range shown along the Y axis. There is a linear relationship between S_D and S over the full gray scale range. In (B) the image is narrowly windowed to place the signals from P and Q at the lower and upper ends of the S_D range shown on the Y axis. The contrast between P and Q (difference in signal level shown on the Y axis) is increased in (B) compared with (A). In (B) signal values less than P on the X axis are all shown at the lowest signal level on the Y axis, and signal values along the X axis greater than Q are all shown at the highest signal level on the Y axis (horizontal lines). In these regions, voxels have the same signals and show no contrast between them. They form isointense blocks and anatomical detail is lost within the blocks. (C) plots signal against T_1 using a dSIR bipolar T_1-filter. Contrast between P and Q is high in the mD as in (B). Values of T_1 less than P and greater than Q do not form plateaux as in (B) but follow the bipolar T_1-filter in the lD and hD. There are therefore differences in signal between voxels so contrast is maintained and anatomical detail is preserved outside of the mD bounded by P and Q.

Methods

With approval from the New Zealand Health and Disability Ethics Committee 20/CEN/246 (26 June 2020), 21/CEN/246 (1 May 2021); 20/NTB/14 (21 May 2020); UAHPEC 018466 (20 Dec 2019); and the Northern B Health and Disability Ethics Committee 2022 EXP 13106 (18 Nov 2022) as well as informed consent from each subject, MR scans were performed on four adult normal controls, seven adult patients with mild traumatic brain injury (mTBI), MS, methamphetamine substance use disorder, Grinker's myelinopathy, Parkinson's disease and white matter in a patient with a glioma. The research was conducted in accordance with the Declaration of Helsinki. 3T scanners (General Electric Healthcare Premier and Siemens Healthineers Skyra) were used. 2D IR FSE sequences were performed with a TI_s chosen to null the shortest T_1 normal white matter (or slightly shorter) and a longer TI_l chosen to produce narrow mD dSIR images targeted at small increases in the T_1 of white matter from normal as illustrated in Figure 6C. 3D wide mD dSIR images with a short TI_s and a long TI_l were also obtained [5]. Longer TE 2D IR images were acquired to produce cdSIR images. Positionally matched 2D and 3D T_2-FLAIR images were obtained as well as susceptibility weighted filtered images as described in Table 1.

 doi:10.20944/preprints202505.2380.v6

Table 1. Pulse sequences and pulse sequence parameters. Only 2D scans were performed on the Siemens Healthineers Skyra system.

#	Sequence	TR (ms)	TI (ms)	TE (ms)	Matrix size Voxel size (mm)	Number of slices	Slice thickness (mm)
1*	2D IR FSE (for white nulling matter)	5,796	350	7	256 x 224 0.9 x 1.0 Z512 0.4 x 0.4	26	4
2*	2D IR FSE (used with #1 for narrow mD dSIR)	5,796	500	7	256 x 224 0.9 x 1.0 Z512 0.4 x 0.4	26	4
3*	2D IR FSE (for longer T_1 nulling)	5,796	600	7	256 x 224 0.9 x 1.0 Z512 0.4 x 0.4	26	4
4*	2D IR FSE (used with #1 for wide mD dSIR)	5,796	800	7	256 x 224 0.9 x 1.0 Z512 0.4 x 0.4	26	4
5	3D BRAVO (for white matter nulling)	2,000	400	6	256 x 256 0.8 x 0.8 Z512	220	0.8
6	3D BRAVO (used with #5 for wide mD dSIR)	2,000	800	6	256 x 256 0.8 x 0.8 Z512	220	0.8
7*	2D T_2-FLAIR	6,300	1,851	102	320 x 240 0.7 x 0.7 Z512 0.4 x 0.4	26	4
8	3D T_2-FLAIR	6,300	1,850	102	256 x 256 0.8 x 0.8 Z512 0.6 x 0.6	252	0.8
9	3D susceptibility weighted	40	-	32	300 x 300 0.8 x 0.8 Z512	110	2

Z = zipped

* = positionally matched for slice position, slice thickness, slice number, field of view and interpolated matrix size

Illustrative Cases

Mild Traumatic Brain Injury (mTBI)

 doi:10.20944/preprints202505.2380.v6

Conventional MRI images usually show little or no change in mTBI but narrow mD dSIR images frequently show extensive high signal areas in white matter (the whiteout sign) (Figure 1). This may resolve within as little as two days or persist over years. It is generally attributed to neuroinflammation but oedema, demyelination and degeneration may also have a role.

In addition to the whiteout sign, there may be loss of contrast in the gray matter of the thalamus due to an increase in T_1. This is manifest as a low contrast appearance between the medial and lateral thalamus (Figure 12A) (arrows) (a grayout sign). After remission normal high gray white matter contrast is restored (Figure 12B) (arrows). Contrast between the lateral thalamus (arrows) and the posterior limb of the internal capsule (PLIC) is low in (Figure 12A) but very high in (Figure 12B). The low contrast between the thalamus and the PLIC in (A) results from a reduction in signal in the gray matter of the lateral thalamus due to an increase in its T_1 in the hD as well as an increase in signal in the white matter of the PLIC due to an increase in its T_1 in the mD. This is reversed in (Figure 12B) where the normal high contrast boundary is restored.

Figure 13A shows a normal control with obvious contrast between the heads of the caudate nuclei and the adjacent CSF as well as between the cortex and CSF. Figure 13B shows a patient with mTBI who has a whiteout sign. There are grayout signs in the thalamus and putamen. In addition, contrast is lost between the heads of the caudate nuclei and CSF as well as between cortex and CSF which appear isointense. These are grayout signs. Thus, the patient has a combination of whiteout and grayout signs.

There may also be gray matter changes elsewhere in mTBI. The normal red nuclei have relatively short T_1s resulting in their normal signal being mid-gray in the mD (arrows) (Figure 14A). They shows a higher signal due to increase in T_1 in a case of mTBI (arrows) (Figure 14B).

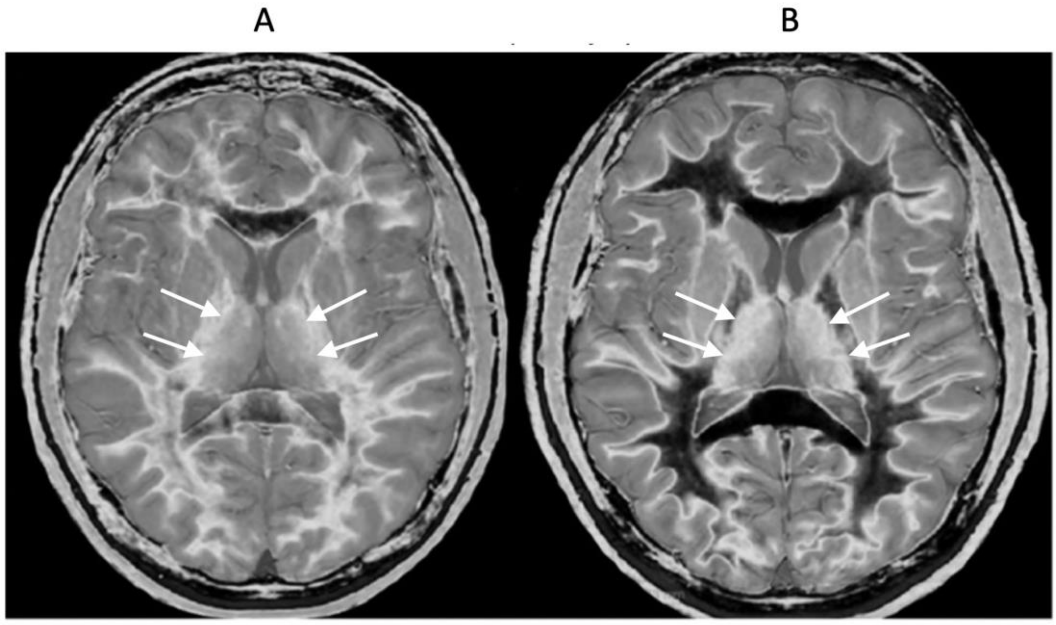

Figure 12. 18-year-old patient with mTBI 21h (A) and 64h (B) post injury imaged with the same narrow mD dSIR (T_1-BLAIR) sequence. In (A) the patient shows a whiteout sign (grade 4 out of 5) with high signal in most of the white matter in the cerebral hemispheres except for the anterior and posterior central corpus callosum. The posterior limb of the internal capsule is high signal. The thalami show low internal contrast from medial to lateral (arrows on lateral margins of the thalami). There is also low external contrast between the lateral margins of the thalami and the adjacent posterior limbs of the internal capsule.On the follow up examination at 64h (B) the whiteout sign has resolved with low signal now in the white matter including the posterior limbs of the internal capsule (except for the corticospinal tracts). The thalami now show high internal contrast from medial to lateral (arrows on lateral margins of the thalamus) which is the normal appearance at this age. There is now also very

 doi:10.20944/preprints202505.2380.v6

high external contrast between the lateral margin of the thalamus and the adjacent posterior limb of the internal capsule. Image (A) shows the grayout sign which is a reduction in the high contrast between the medial and lateral gray matter of the thalamus. The high contrast is restored in (B). No abnormality was seen on the corresponding T_2-FLAIR images obtained at both time points.

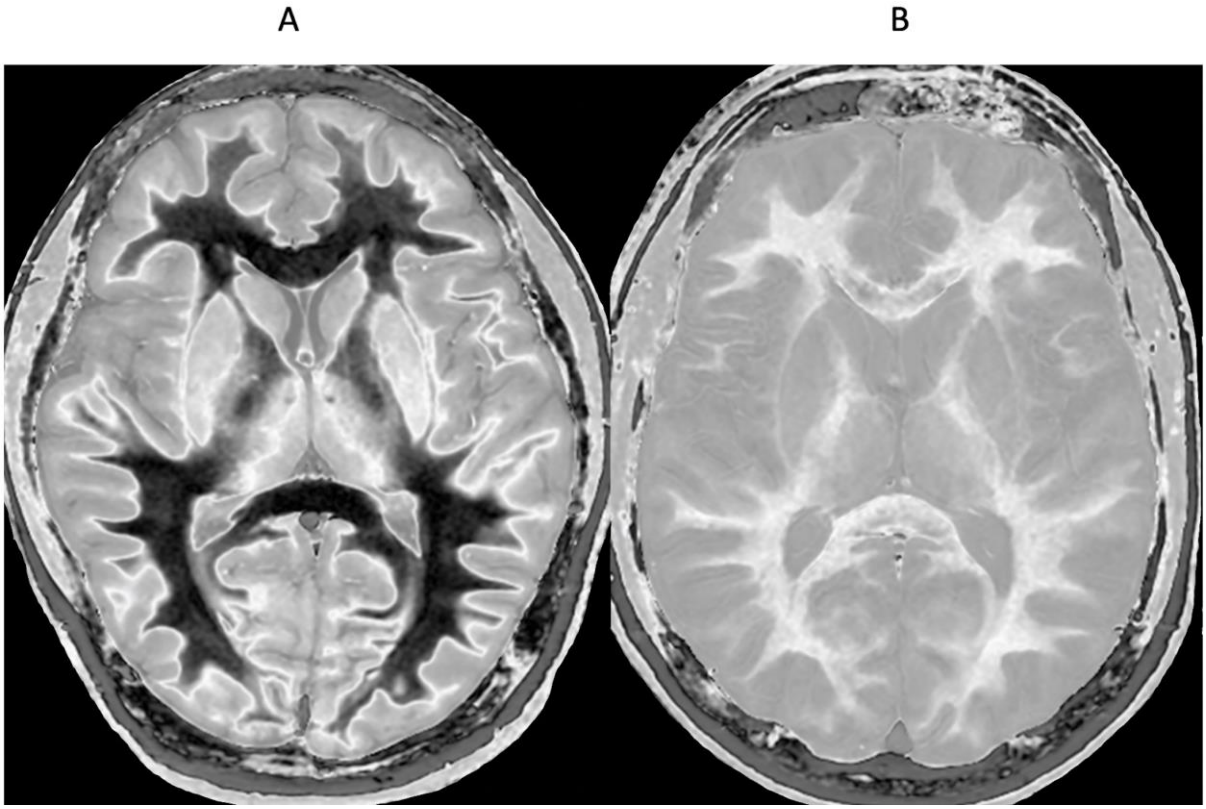

Figure 13. Normal control (A) and patient with mTBI (B) showing a whiteout sign and grayout signs (narrow mD dSIR [T_1-BLAIR] images). The normal control shows the heads of the caudate nuclei with higher signal than the adjacent CSF. Contrast is also seen between the cortex and CSF. In (B), the patient shows a whiteout sign. There are grayout signs in the thalami and putamina. In addition, contrast between the heads of the caudate nuclei and CSF is reduced and there is little or no contrast between cortex and CSF which are isointense. These are also grayout signs. No abnormality was seen on the T_2-FLAIR images in the normal control or patient.

 doi:10.20944/preprints202505.2380.v6

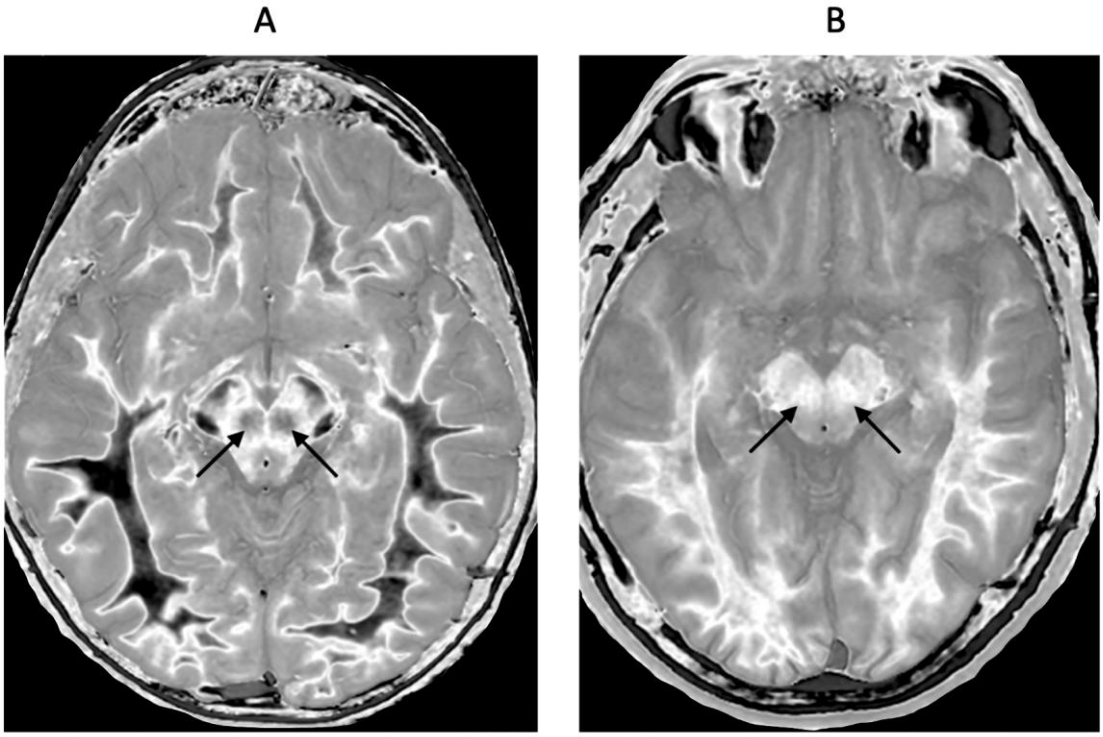

Figure 14. Red nuclei in an 18-year-old normal control (A) and an 18-year-old male patient with mTBI (B). 2D narrow mD dSIR (T_1-BLAIR) images. In (A) the normal control shows low signal in the white matter of the cerebral hemisphere, cortico-spinal tracts and the ascending sensory tracts. The red nuclei (arrows) have an intermediate mid-gray signal. In (B) the patient shows high signal in the cerebral white matter, the corticospinal tracts and the ascending sensory tracts (whiteout sign, grade 4 out of 5). In addition, the red nuclei are higher signal than in (A) (arrows). No abnormality was seen on the T_2-FLAIR images in the normal control or patient.

Multiple Sclerosis (MS)

Focal lesions, as well as patchy white matter changes, may be seen in areas that appear normal on T_2-wFSE images in a patient in remission (Figure 15) (compare with normal low signal appearance of normal peripheral white matter in Figure 1B). In another case during a relapse, one lesion is seen on the T_2-FLAIR image in Figure 16A (long arrow). This lesion is also seen in Figure 16B (long arrow). There are an additional six lesions (small arrows) in Figure 16B. Five of the lesions in Figure 16B have high signal boundaries. This can be due to a large increase in T_1 in the lesion beyond the peak of the bipolar T_1-filter or a decrease in the abnormal T_1 in the lesion due to the presence of paramagnetic free iron. Two of the lesions with high signal boundaries shown in Figure 16B have paramagnetic rim signs on the filtered susceptibility weighted images (arrows, Figure 16C). The high signal boundaries seen on some MS lesions may be a sign of disease activity.

In addition, there are widespread abnormal areas in white matter which are only seen on the dSIR images (Figure 16). These changes are typically bilateral, symmetrical and have an increased signal. They have the features of a whiteout sign (Figure 16B) and to date have only been seen in patients with MS during a relapse.

Composite T_1 and T_2 cdSIR images may show higher contrast than corresponding dSIR images (Figures 17A and 17B).

In the spinal cord in another patient diagnosed with MS, the T_2-FLAIR image only shows an ill-defined smudge (arrow) (Figure 18A). The corresponding wide mD dSIR image (Figure 18B) shows an extensive, well defined, high contrast abnormality (arrows). Another lesion is seen in the medulla on the dSIR image (arrow) but not on the T_2-FLAIR image.

 doi:10.20944/preprints202505.2380.v6

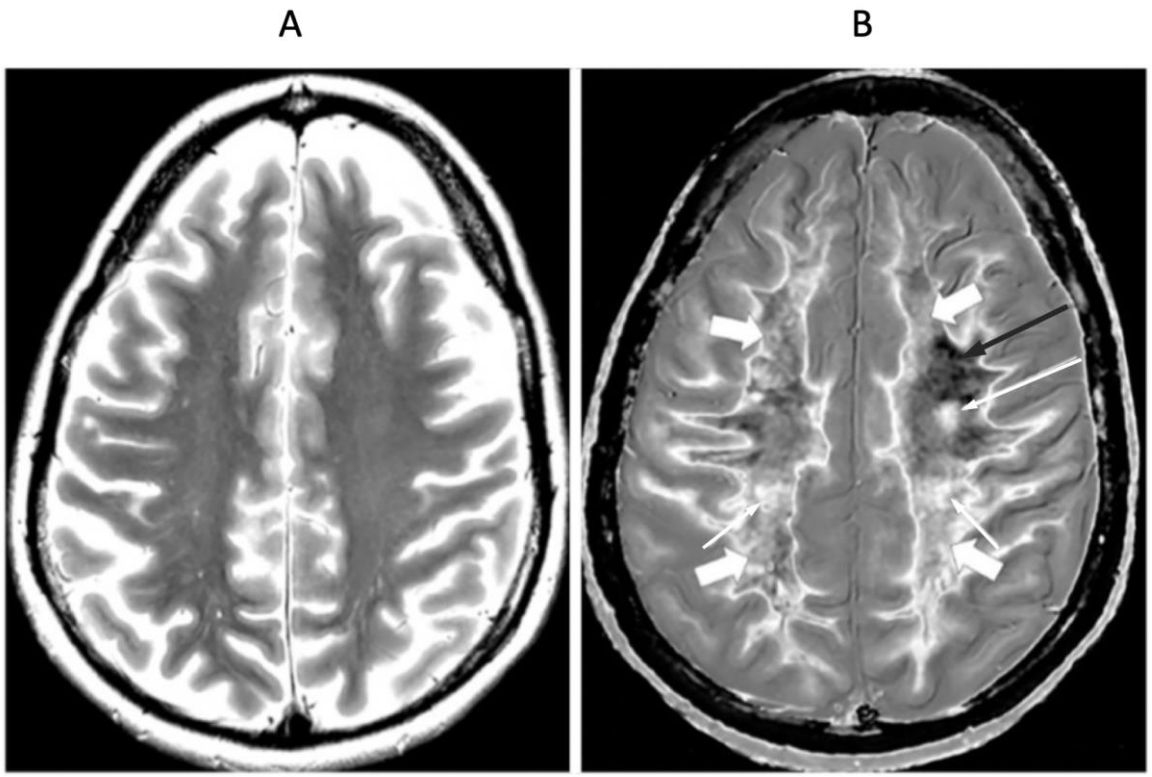

Figure 15. 41-year-old female patient with MS in remission. 2D T_2-wSE (A) and narrow mD dSIR (T_1-BLAIR) (B) images at the same level. No abnormality is seen in (A). A focal lesion is seen in (B) (long narrow white arrow) and the cortico-spinal tracts show a high signal (short narrow white arrows). In addition there is patchy increased signal in white matter (short thick white arrows) with only a small region showing a normal or near normal low signal appearance (long black arrow). High contrast and high spatial resolution contrast are seen at the boundaries between normal white matter and normal gray matter in (B). These features are less obvious in areas where the white matter has abnormal high signal.

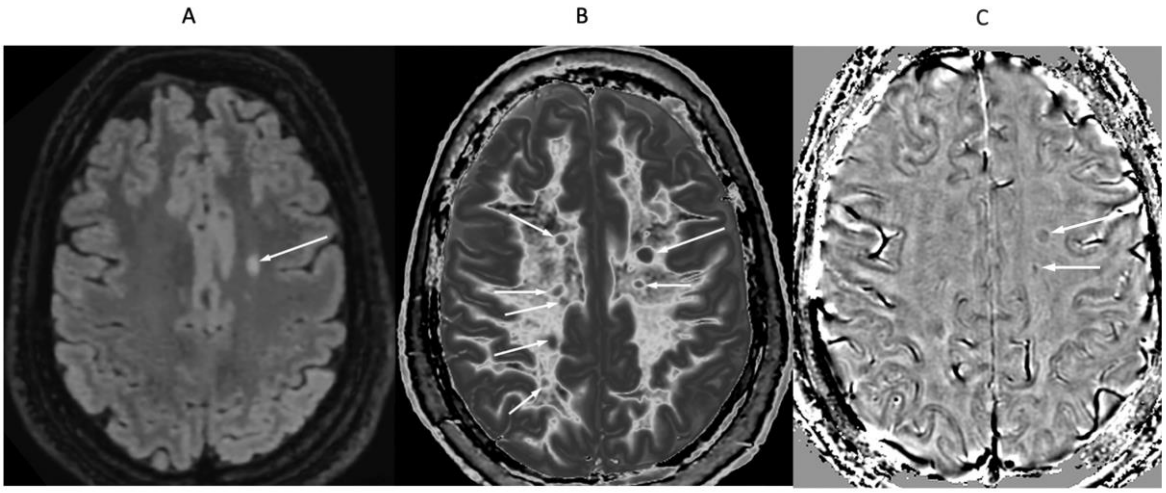

Figure 16. 32-year-old female with MS during a relapse. T_2-FLAIR (A), synthetic narrow mD dSIR (T_1-BLAIR) (B) and filtered gradient echo (C) images. On the T_2-FLAIR image (A), one lesion is seen (long arrow). The surrounding white matter appears normal. On the T_1-BLAIR image (B), the lesion shown on the T_2-FLAIR image is seen with a high signal boundary (long arrow) as well as six other lesions four of which also show high signal boundaries or bubble signs (short arrows). Two of the five high signal lesions show paramagnetic rim signs on the filtered gradient echo image (arrows) in (C). In addition, most of the white matter in (B) is high signal corresponding to a high grade 4/5 whiteout sign [1]. No whiteout sign is seen on the T_2-FLAIR image (A).

 doi:10.20944/preprints202505.2380.v6

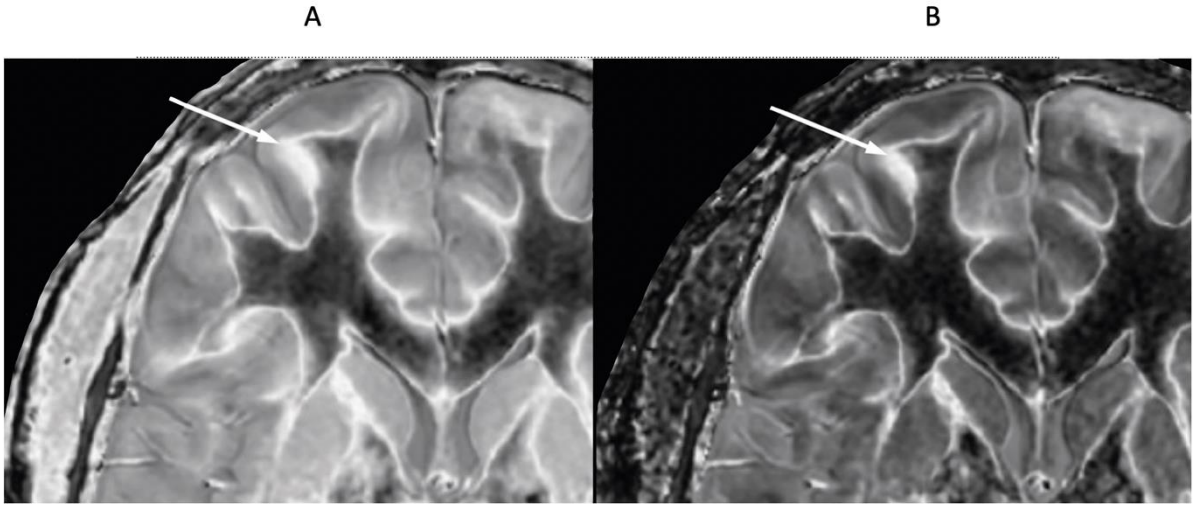

Figure 17. 24-year-old female patient with MS in remission (TI_s = 350 ms, TI_i = 500 ms). Narrow mD dSIR (T_1-BLAIR) (A) and composite (T_1 and T_2) cdSIR (TI_s/TE_s = 350/7 and 80 ms; TI_i/TE_i = 500/7 ms) (T_1,T_2-BLAIR) (B) images. A leukocortical lesion is seen on the T_1-BLAIR image (A) and with higher contrast on the T_1,T_2-BLAIR image in (B) (arrows). White matter and gray matter boundaries are higher contrast and narrower on the composite filter cdSIR image (B). Also white matter is more uniformly low signal in (B). These features are consistent with the attenuation of the first IR TI_s filter signal increasing contrast and narrowing boundaries at the positive pole and decreasing these at the negative pole as shown in Fig. 10A.

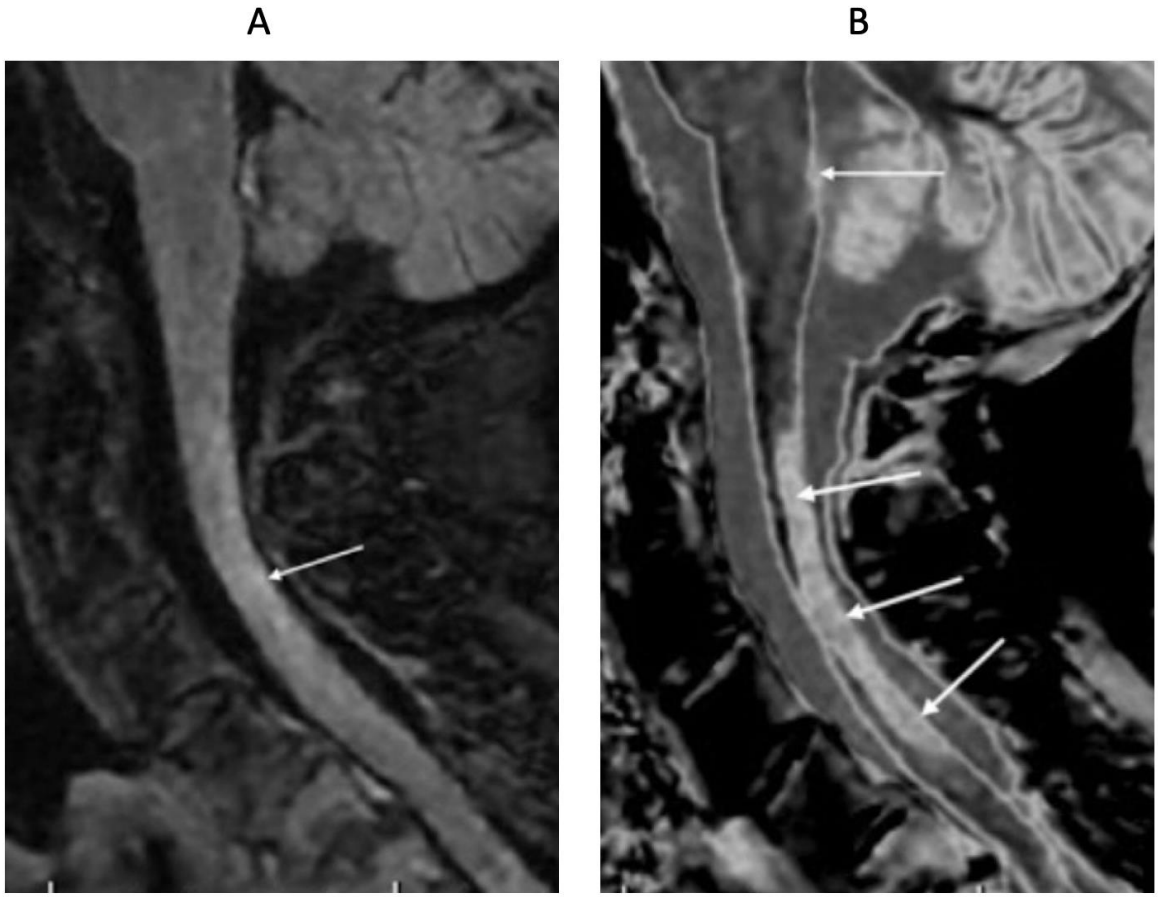

Figure 18. 76-year-old female patient in remission with a diagnosis of MS. Sagittal 3D T_2-FLAIR (A) and 3D wide mD dSIR (T_1-BLAIR) (B) images. The T_2-FLAIR image shows a poorly defined area of increased signal in the

 doi:10.20944/preprints202505.2380.v6

cervical cord (arrow). The T_1-BLAIR image shows a high contrast lesion with sharply defined ("punched out") boundaries in the cervical cord (lower three arrows). This is much more extensive than in (A). An additional lesion is seen in the medulla on the T_1-BLAIR image in the region of the area postrema (highest arrow) (B) but not on the T_2-FLAIR image (A). The extended lesion in the cervical cord and the lesion in the area postrema raise the possibility of neuromyelitis optica spectrum disorder. Other conventional sequences such as T_2-wSE or STIR may perform better than T_2-FLAIR in the cervical cord.

Methamphetamine Substance Use Disorder

Patients with methamphetamine substance use disorder may show a heterogenous pattern of white matter abnormalities with dSIR sequences but they may also show clearly defined whiteout signs and these can remit with continued abstinence (Figure 19) (compare with normal appearance in Figure 1B). The situation may be confounded in the case shown by a previous mTBI.

Delayed Post-Hypoxic Leukoencephalopathy (Grinker's Myelinopathy)

This is thought to be a rare syndrome in which classically patients make an initial recovery after a hypoxic and/or ischaemic episode, and then deteriorate with severe neurological signs such as Parkinsonism and akinetic mutism. Conventional MRI shows widespread abnormalities in the white matter of the cerebral hemispheres. In post-hypoxic patients, it is possible to see extensive abnormalities in white matter with dSIR sequences where no abnormalities are seen with conventional sequences [7]. The patients typically have cognitive symptoms of less severity than those included in classical descriptions. This less severe form of Grinker's myelinopathy may be much more common than the classical form but not be recognised radiologically using conventional MRI sequences.

Parkinson's Disease

Parkinson's disease may show more obvious bilaminar signs in the cortex than in age matched controls (i.e., an increase in signal in the outer layer of the cortex) with narrow mD dSIR sequences (white arrows) (Figure 20). The inner higher signal is from the boundary between white matter and gray matter and the next layer outwards is lower signal in the inner cortex. The next outer layer beyond this is the higher signal layer in the outer cortex.

Bubble signs in which circular areas of similar size are seen in the gray matter in the basal ganglia and thalamus can also be seen (e.g., black arrows) (Figure 20).

White Matter Associated with Cerebral Tumours

In cases of cerebral tumours, extensive white matter changes have been seen after chemotherapy in areas that appeared normal on T_2-FLAIR images (Figure 21A and 21B). When typical radiation or chemotherapy changes have been seen on T_2-FLAIR images, additional changes have been observed in the form of whiteout signs.

Normal Control and MS Patient with dSIR and lSIR Images

dSIR and lSIR images (Figs. 22A and 22B) are compared in a 46-year-old male normal control. White matter-gray matter boundaries and the bilaminar cortex sign (arrows) are seen with higher contrast and higher spatial resolution on the lSIR image. Bubble signs are also better seen in the thalamus and putamen on the lSIR image. A small decrease in T_1 through the sharp peak of the lSIR bipolar T_1-filter results in finer boundaries and narrower margin bubble signs with the lSIR bipolar T_1-filter compared to the dSIR bipolar T_1-filter.

In a 41-year-old female patient with MS, the dSIR image (Figure 23A) shows a blurred leukocortical lesion in the right medial frontal region with no evidence of a white matter-gray matter boundary within it. The matched lSIR image (Figure 23B) shows a disrupted high signal boundary between white matter and gray matter within the lesion. Profiles (plots of signal against position in mm) through the lesion at the level shown by the arrows for the dSIR (blue) and lSIR (orange) images shows a higher signal and steeper slope for the lSIR image (Figure 23C). The spatial resolution of the contrast i.e., change in signal with change in position is generally higher on the lSIR image

 doi:10.20944/preprints202505.2380.v6

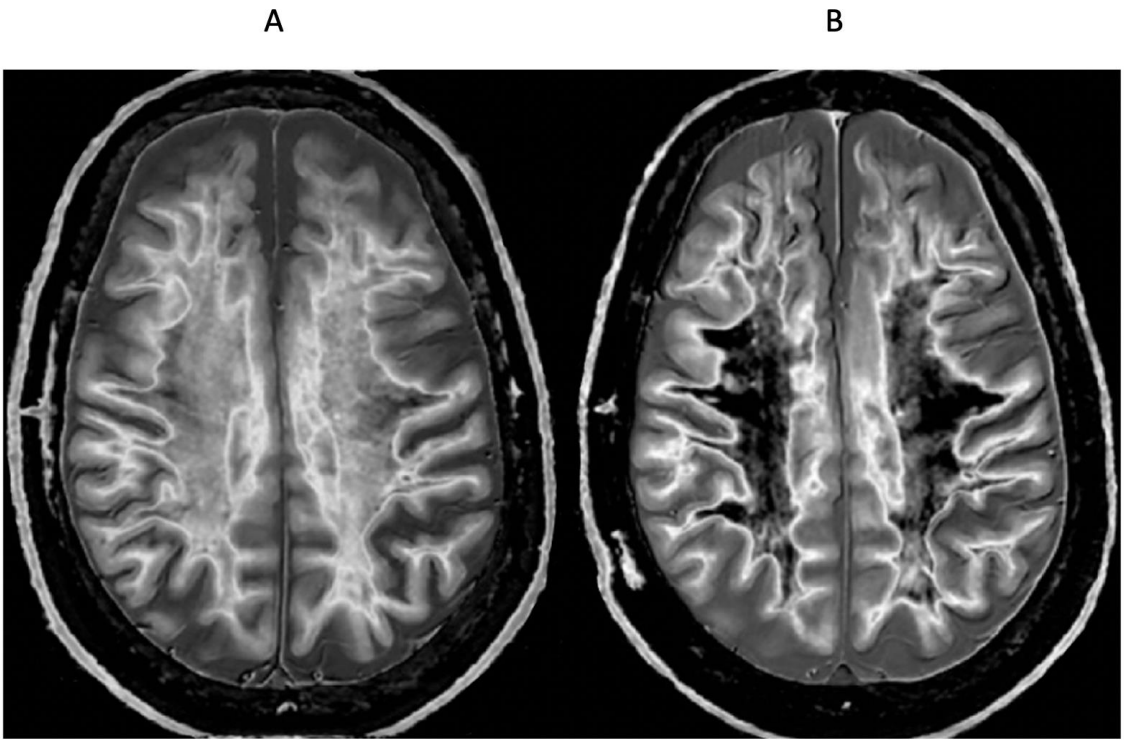

Figure 19. 51-year-old male patient with methamphetamine substance use disorder after one month's abstinence (A) and after nine months' abstinence (B). Positionally matched narrow mD dSIR (T_1-BLAIR) images. In (A) there is extensive high signal in the white matter of the cerebral hemispheres with only small areas of normal or near normal white matter (dark) at the periphery of the white matter (whiteout sign, grade 4 out of 5). After nine months' abstinence (B), the high signal areas in (A) have markedly regressed. There is some intermediate signal in the more central white matter and lower signal in the peripheral white matter (whiteout sign grade 2 out of 5, where grade 1 is normal). No abnormality was seen in either examination on the corresponding T_2-FLAIR images. A previous mTBI in the patient may have been a confounder.

 doi:10.20944/preprints202505.2380.v6

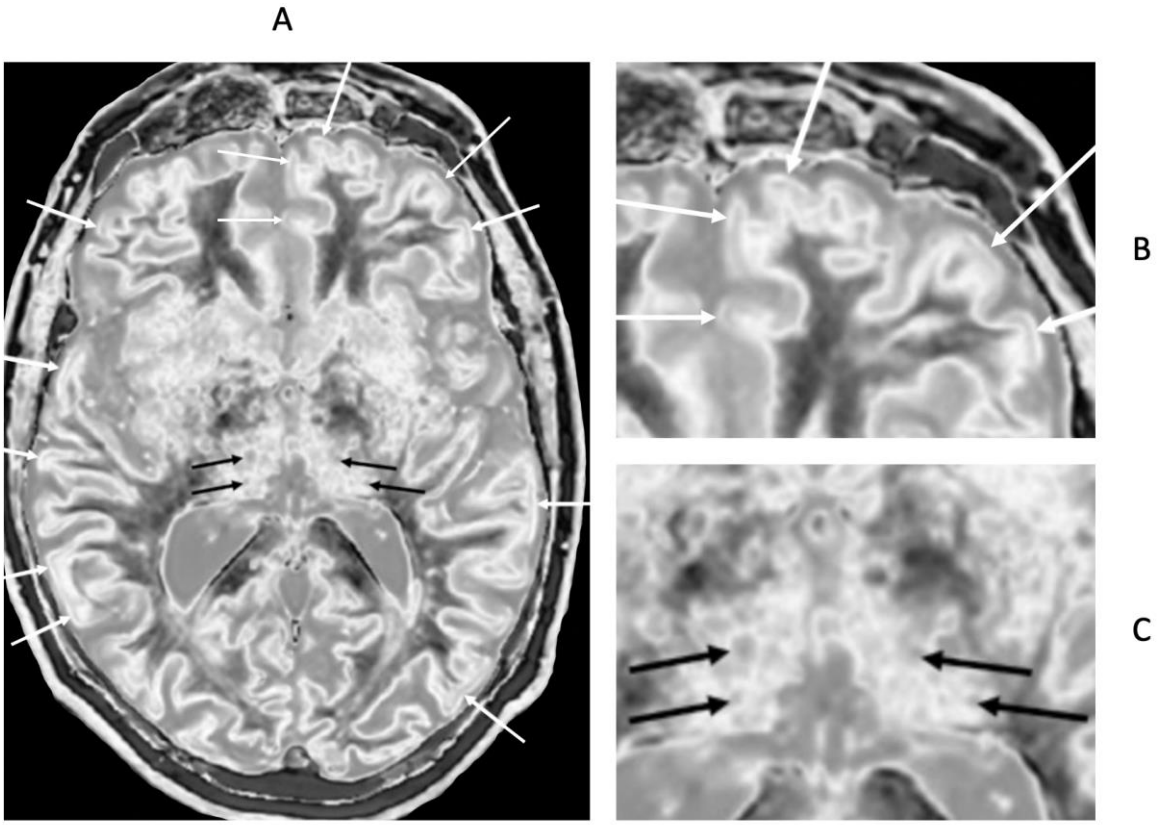

Figure 20. 72-year-old male patient with Parkinson's disease. 2D narrow mD dSIR (T_1-BLAIR) image (A) with insets of anterior left cortex (B) and thalami (C). There is high signal in the superficial layer of the cortex at multiple sites (bilaminar cortex signs) which are more obvious on the inset (white arrows) (B). There are circular appearances in the thalami, putamen and heads of the caudate nuclei (bubble signs) which are more obvious on the inset (e.g., black arrows) (C). The bubble sign is due to focal reductions in T_1 probably from the presence of free iron. The thalamic signal is slightly higher medially compared with laterally unlike the appearance of the normal thalamus in the 18-year-old patient shown in Fig. 12B.

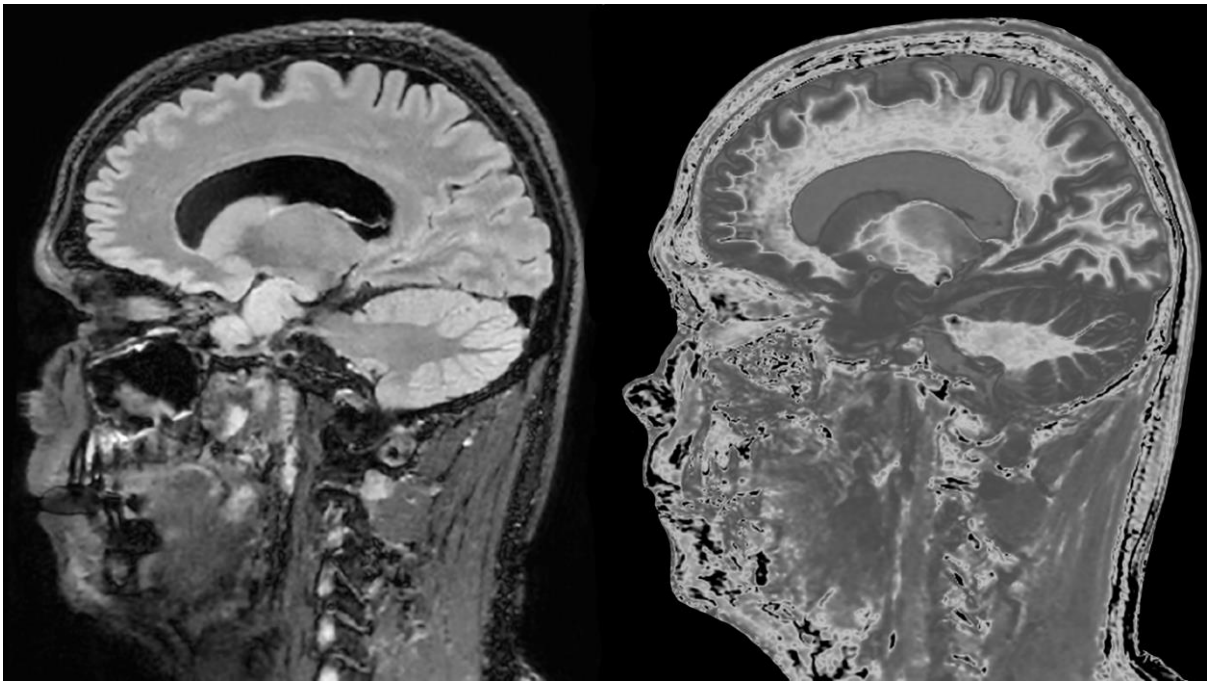

 doi:10.20944/preprints202505.2380.v6

Figure 21. 65-year-old female with a glioma (not shown) post chemotherapy. Parasagittal T_2-FLAIR (A) and synthetic narrow mD dSIR (T_1-BLAIR) (B) images. On the T_2-FLAIR image no abnormality is seen. On the T_1-BLAIR image (B), the white matter has a high signal corresponding to a high grade whiteout sign. This includes the cerebellar white matter which is similar in intensity to the cerebral white matter. There is some sparing of the peripheral white matter in (B).

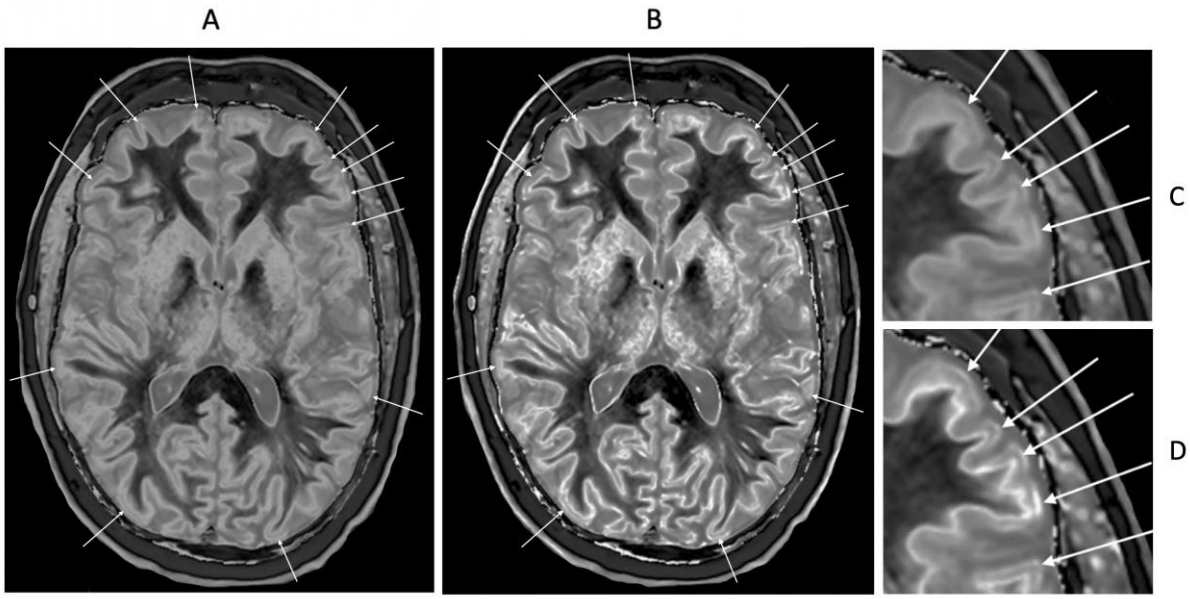

Figure 22. 46-year-old normal control. Narrow mD dSIR (A) and narrow mD lSIR (B) T_1-BLAIR images with insets of anterior left cortex dSIR in (C) and anterior left cortex lSIR in (D). The boundaries between white matter and gray matter are seen with higher contrast and the contrast is seen with higher spatial resolution in (B) and (D) compared with (A) and (C). Bilaminar cortex signs are also seen with higher contrast and spatial resolution in (B) and (D) (white arrows). There are also small bubble signs in the putamen and medial thalamus which are better seen on the lSIR image (B) compared with the dSIR image (A).

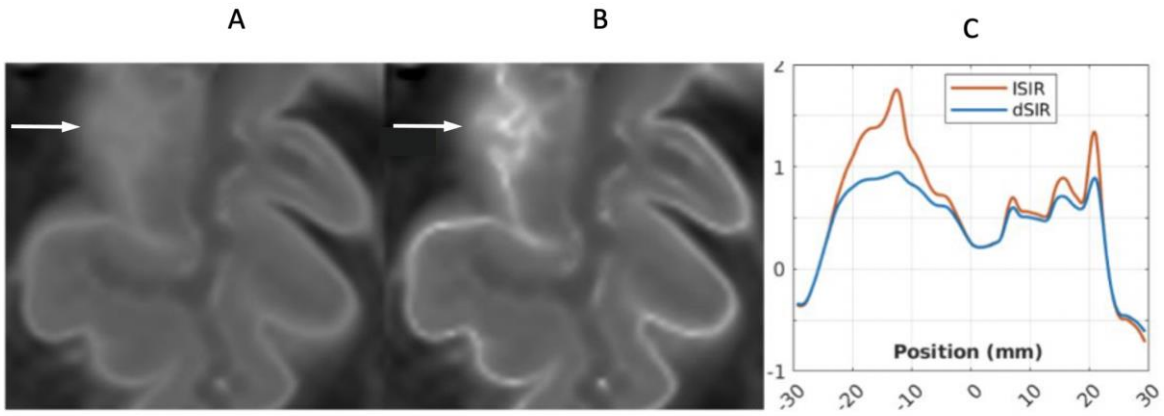

Figure 23. 41-year-old female patient with MS. A leukocortical lesion in the right medial frontal region is shown on the narrow mD dSIR (T_1-BLAIR) image (A) and a matching lSIR image (B) (arrows). There are also left to right profiles with signal plotted against position (in mm) for the dSIR (blue) and lSIR (orange) images (C) at the level of the horizontal arrows shown in (A) and (B). No boundary between white matter and gray matter is seen within the lesion in (A). A disrupted high signal boundary between white matter and gray matter is seen in the lesion in (B). The lSIR profile (orange) has higher signal and steeper slopes than the dSIR profile (blue) in (C).

 doi:10.20944/preprints202505.2380.v6

The difference in signal (or contrast) achieved for the same change in position is generally greater with the lSIR filter i.e., the contrast shown on the lSIR image generally has a higher spatial resolution.

Discussion

UHC MRI using Bipolar Filters

UHC MRI is a term used to describe MRI techniques which show much greater contrast than conventional state-of-the-art MRI images while having similar spatial resolutions and comparable acquisition times. This is achieved with no increase in static or gradient magnetic field. UHC MRI using bipolar filters employs sequences which exist on most MRI machines together with minimal image processing. It can be implemented in a very short time at very little cost.

UHC MRI is distinguished from ultra-high field MRI which uses static magnetic field strengths of 7T or higher to improve image signal-to-noise ratio. This improvement may be used to increase contrast, spatial resolution and/or the speed of MRI scans [11-15].

UHC MRI is also distinguished from ultra-high spatial resolution MRI where typically increased gradient strength is used to improve spatial resolution [16,17].

The four groups of BLAIR sequences discussed in this paper are summarised in Table 2 including some of their variants and the dominant source(s) of contrast for each sequence. The sequence signal equations and other relevant functions are included in Table 3. The Tables also provide information for instituting synthetic imaging although relevant MT effects may need to be added.

Table 2. Four types of directly acquired BLAIR sequences and their tissue properties. The fourth column shows the dominant source(s) of contrast for each sequence in their common mode(s) of use.

BLAIR sequence	**Reverse subtracted BLAIR sequence**	**Tissue properties**	**Dominant source(s) of contrast - BLAIR**
†DIR	-	ρ_m, T_1, T_2, ±MT	T_1,T_2-BLAIR
lDIR	-	ρ_m, T_1, T_2, ±MT	T_1,T_2-BLAIR
†SIR	rSIR	ρ_m, T_1, T_2, ±MT	T_1,T_2-BLAIR
ENVI	-	ρ_m, T_1, T_2, ±MT	T_1,T_2-BLAIR
†dSIR	drSIR	T_1, ±MT	T_1-BLAIR
cdSIR	cdrSIR	T_1, ±T_2, ±T_2*, ±D*, ± χ, ±MT	T_1,T_2-BLAIR, etc
†lSIR	lrSIR	T_1, ±MT	T_1-BLAIR
clSIR	clrSIR	T_1, ±T_2, ±T_2*, ±D*, ± χ, ±MT	T_1,T_2-BLAIR, etc

† main sequences.

 doi:10.20944/preprints202505.2380.v6

Table 3. Signal equations for bipolar filters and other functions.

#	Filter, other functions	Signal Equation	Fig. #
1	IR, TI_s	$S_{TIs} = 1\text{-}2e^{-TIs/T_1}$	3,4,5
2	IR, TI_i	$S_{TIi} = 1\text{-}2e^{-TIi/T_1}$	3,4,5
3	DIR, TI_l, TI_s	$S_{DIR} = \rho_m\,(1\text{-}2e^{-TIl/T_1})\,(1\text{-}2e^{-TIs/T_1})\,e^{-TE/T_2}$	26
4	SIR	$S_{SIR} = S_{TIs} - S_{TIi}$	5
5	dSIR	$S_{dSIR} = \frac{S_{TIs} - S_{TIi}}{S_{TIs} + S_{TIi}} \quad \left(\frac{\text{difference}}{\text{sum}}\right)$	6,9
6	dSIR	$S_{dSIR} \approx \frac{\Delta TI}{T_1\left(e^{TI/T_1} - 2\right)} \quad \left(\frac{\text{difference}}{\text{sum}}\right)$ (in lD and hD) $\Delta TI = TI_i - TI_s$ $S_{dSIR} \approx \frac{T_1\left(e^{TI/T_1} - 2\right)}{\Delta TI} \quad \left(\frac{\text{sum}}{\text{difference}}\right)$ (in mD)	6,9
7	cdSIR	$S_{dSIR} = \frac{S_{TIs} \cdot S_{OF} - S_{TIi}}{S_{TIs} \cdot S_{OF} + S_{TIi}} \quad S_{dSIR} = \frac{S_{TIs} - S_{TIi} \cdot S_{OF}}{S_{TIs} + S_{TIi} \cdot S_{OF}}$	10
8	cdSIR, S_{OF}	$S_{OF} = \pm e^{-\Delta TE/T2}, \pm e^{-\Delta TE/T2^*}, \pm e^{-\Delta bD^*}$, etc	10
9	dSIR, S_{dSIR}	$S_{dSIR} \approx \frac{\ln 4}{\Delta TI} T_1 - \frac{\Sigma TI}{\Delta TI}$ (in mD)	6
10	dSIR, T_1	$T_1 \approx \frac{\Delta TI}{\ln 4} S_{dSIR} + \frac{\Sigma TI}{\ln 4}$ (in mD)	6
11	lSIR	$S_{lSIR} = \frac{1}{2}(\ln S_{TIs} - \ln S_{TIi})$	8,9
12	clSIR	$S_{lSIR} = \ln S_{Tis} \cdot S_{OF} - \ln S_{TIi} \quad S_{lSIR} = \ln S_{Tis} - \ln S_{TIi} \cdot S_{OF}$	
13	clSIR, lSIR	$S_{clSIR} = S_{lSIR} \pm \frac{\Delta TE}{T_2}, \pm\frac{\Delta TE}{T_2^*}, \pm\Delta bD^*$, etc	
14	lSIR, dSIR†	$S_{lSIR} = \text{atanh}\, S_{dSIR}$ (in mD)	9
15	dSIR ††	$\frac{dS_{dSIR}}{dT_1} \approx \frac{\ln 4}{\Delta TI}$ (in mD)	6,9
16	lSIR †††	$\frac{dS_{lSIR}}{dT_1} \approx \frac{\ln 4}{\Delta TI} \bullet \frac{1}{\left(T_1 - \frac{TIs}{\ln 2}\right)} \bullet \frac{1}{\left(T_1 - \frac{TIi}{\ln 2}\right)}$ (in mD)	9

 doi:10.20944/preprints202505.2380.v6

† S_{ISIR} is the inverse hyperbolic tangent of S_{dSIR} in the mD. †† $\frac{dS_{dSIR}}{dT_1}$ is the T_1 derivative of S_{dSIR} and gives the slope of the dSIR T_1-filter in the mD which is essentially constant and equal to $\frac{\ln 4}{\Delta TI}$ (Fig. 9). ††† $\frac{dS_{lSIR}}{dT_1}$ is the T_1 derivative of the S_{ISIR} T_1-filter in the mD which varies. It has values of minus or plus infinity when $T_1 = \frac{TI_s}{\ln 2}$ and $T_1 = \frac{TI_i}{\ln 2}$ respectively (Fig. 9).The dSIR sequence is the BLAIR sequence most used in the present studies. T_1 measurements obtained with it have been validated in quantitative phantom and human studies [18-20].

While the emphasis in this paper has been on white matter in the mD and grey matter in the hD, very high contrast can also be seen in the central grey matter of the brain when this is in the mD rather than in the hD. In addition, iron containing tissues have only been studied with dSIR using the single tissue property T_1, not the composite sequence cdSIR using the two tissue properties T_1 and T_2*.

Understanding the contrast produced by bipolar TP-filter sequences is greatly helped by use of their TP-filters. These filters relate differences or changes in tissue properties to contrast using their slopes and explain signal and contrast patterns that can otherwise appear inexplicable using conventional approaches [8,9].

Artefacts from too high a value of TI_i, misregistration, partial volume effects and other causes are described in reference [5]. Means of avoiding these and/or reducing their effects are included in reference [5].

Tissue and Fluid Boundaries

dSIR and lSIR images are characterised by sharply defined high contrast, higher spatial resolution boundaries between white matter and gray matter as well as between white matter and CSF, and between gray matter and CSF. The site of the boundaries as well as their width can be changed by varying the TIs of the sequence [5]. The boundaries are specific and located at iso-T_1 contours. They are not part of a generalised pattern of edge enhancement.

In addition, there are well defined low signal (dark) boundaries between white matter, gray matter and CSF as modelled by bipolar TP-filters.

High signal in-plane boundaries on dSIR images usually have a uniform and consistent appearance although these are subject to partial volume effects and may simulate lesions particularly with 2D images acquired with relatively thick slices (e.g., 2-4 mm). Through-plane partial volume effects also produce high signal from boundaries and these are more prominent with thick slices.

A systematic treatment of boundaries including variation in signal with position using TP-filters, the partial derivative change in T_1 with tissue fraction and the partial derivative change of tissue fraction with position is described in reference [5]. Using this approach, differences in signal (i.e., contrast) can be related to differences in position within the boundary region.

Hybrid Quantitative and Qualitative Imaging

dSIR sequences produce single images that can be used both quantitatively and qualitatively. The images show high contrast and this can be used for conventional qualitative image interpretation. The dSIR images are also T_1 maps so they can be used to directly measure T_1 values in regions of interest placed on them for quantitative studies. In comparison with the conventional approaches to T_1 quantitation which use separate images for qualitative interpretation and for T_1 mapping, dSIR images: (i) do not require working with images of two different types; (ii) allow precise placement of ROIs in relation to lesions on the images used for radiological interpretation, and (iii) require no extra time for additional acquisitions.

T_1 values of dSIR sequences have shown comparable accuracy to conventional T_1 mapping in the mD but, as expected, differences in the lD and hD [18-20].

 doi:10.20944/preprints202505.2380.v6

Magnetisation Transfer (MT)

With 2D multislice acquisitions, there may be incidental magnetisation transfer (MT) effects from off-resonance 180° or lower flip angle pulses used during FSE acquisitions. Using two pool modelling, MT decreases the ρ_m observed (ρ_{mobs}) in the free pool but also decreases the observed T_1 (T_{1obs}) of the free pool in proportion to the reduction in ρ_{mobs} [21-27]. This reduction may be quite substantial and decrease normal ρ_{mobs} and T_{1obs} by as much as 50%. In general, MT effects are decreased in disease so the reduction in ρ_{mobs} and T_{1obs} in diseased tissue due to MT is generally less than that in normal tissue. This is manifest as an apparent increase in ρ_{mobs} and T_{1obs} in diseased tissue relative to normal tissue. This is in addition to any increases in ρ_{mobs} and T_1 in diseased tissue for other reasons such as pathological change due to oedema.

2D FSE images with higher echo train lengths (ETLs) require more 180° or similar pulses and thus produce a corresponding increase in MT effects during multislice acquisitions. These produce a greater reduction in values of T_{1obs} and so need shorter nulling TIs. MT effects are less with gradient echo acquisitions as often used with 3D acquisitions. As a result, T_{1obs} may be longer with 3D gradient echo acquisitions than with 2D FSE acquisitions and so their nulling TIs may need to be correspondingly longer. The contrast between normal and abnormal tissues may also be lower with gradient echo acquisitions.

MT can be used intentionally either before or after preparation inversion pulses, as well as both before and after preparation inversion pulses in IR sequences [21]. MT can also be used as an attenuating filter S_{OF} in composite bipolar filters.

Synthetic Bipolar T_1-filters

Synthetic bipolar T_1-filters can be of two types as shown in Table 2. The first uses Eq. 1 and the relationships shown in Figs. 6, 8 and 9 to synthesise dSIR and lSIR images with different TIs from two directly acquired images. The second type uses a synthetic bipolar TP-filter which may be the same or similar to the dSIR and lSIR filters and applies these to tissue property maps. This approach has two aspects: (i) acquiring the tissue property map which should be of high quality in the tissue property Domains or parts of Domains of interest, and (ii) using a visualization function such as a bipolar filter to increase contrast without saturating voxel values. These two aspects are incorporated in directly acquired dSIR and lSIR imaging.

Signs Produced with dSIR Sequences

The Whiteout Sign

This is a generalised bilateral symmetrical increase in signal in white matter of the cerebral and cerebellar hemispheres as well as the brainstem [1]. The increase in signal follows the pattern of normal white matter signals and can involve all, or almost all, of the white matter in a particular slice. It has specific features such as sparing of the anterior and posterior central corpus callosum (genu and splenium) as well as peripheral white matter in the cerebral hemispheres (Figs. 1, 12, 13, 14, 19, 21). The white matter signal can increase up to that of the high signal boundary between white and gray matter and can be divided into five grades with grades 1 and 2 normal and grades 3,4,5 abnormal signs, or alternatively grade 3 as intermediate and grades 4 and 5 as abnormal whiteout signs [1]. It is due to widespread, small increases in T_1 and is thought to be particularly associated with neuroinflammation but may also be due to oedema, demyelination, degeneration and other causes. It has also been seen in mTBI, hypoxic-ischaemic injury to the brain, multiple sclerosis and white matter associated with tumours.

Grayout Signs

With grayout signs there is a loss of contrast in gray matter such as is seen in the thalamus and basal ganglia after mTBI (Figs. 12, 13), or a loss of contrast between gray matter and white matter, or between gray matter and CSF (Figure 13B). Grayout signs are generally more subtle than the whiteout sign. They are associated with an increase in T_1 in gray matter.

 doi:10.20944/preprints202505.2380.v6

In young subjects, the normal lateral thalamus gray matter (TG_{lat}) tends to have a shorter T_1 than the normal medial thalamus gray matter (TG_{med}) (upper horizontal negative solid green arrow). This leads to higher signal in the lateral thalamus with a narrow mD dSIR sequence (first vertical blue arrow) (Figure 24). The T_1 of the lateral thalamus may increase in disease (middle horizontal positive green striped arrow in Figure 24) which produces a loss of contrast with the medial thalamus (blue circle). With reversion back to normal on recovery, the T_1 may decrease back to normal (lowest horizontal negative green arrow) restoring contrast (second vertical blue arrow).

The whiteout sign may be accompanied by grayout signs in conditions such as mTBI as described in this paper. The term post-insult leukoencephalopathy syndromes (PILS) described in reference [1] refers to whiteout signs after mTBI, Grinker's myelinopathy, etc. A term that includes both the whiteout sign and grayout signs as well as the possibility of ongoing effects (rather than just post-insult effects) is reactive encephalopathy (RE). Depending on the observed features (presence/absence of grayout signs), the pattern may be described as PILS/RE. Experimental studies to determine histological origins of the whiteout and grayout signs are in progress.

The Bilaminar Cortex Sign

This is an increase in signal in the outer layer of the cortex which is often barely seen in young adults but becomes more obvious with increasing age as well as in Parkinson's disease. It is seen with narrow mD dSIR images in which there is a high signal at the white matter gray matter junction, a lower signal layer in the inner cortex and a higher signal layer in the outer cortex (Figs. 20, 22). The higher signal generally corresponds to layers I-III and the lower signal to layers IV-VI of the cortex. The increase in signal is usually most obvious at the crest of gyri and to a lesser extent in the banks of sulci. It may be obscured by partial volume effects particularly on 2D images of 4 mm thickness compared with the estimated 2-4 mm thickness of the cortex. The sign may be due to increased free iron content with a decrease in T_1 of the normal cortex with increase in age, with an exaggeration of this in Parkinson's disease [28]. It is distinguished from the double cortex sign [29] which is due to iron deposited in a subcortical location. A bilaminar cortical appearance has been seen with MP2RAGE sequences at 7T after detailed image processing and has been attributed to differences in myelin [30]. The bilaminar cortex sign differs from the high signal that can be seen at the cortical margin on T_2-FLAIR images. This signal is attributed to increased T_2 relative to brain in cortical veins/pia arachnoid (as opposed to a decreased T_1 in the bilaminar cortex sign). It is usually more evident on 2D T_2-FLAIR images with longer TIs and TRs than 3D T_2-FLAIR images though the latter may have very long effective TEs. It can be present in young subjects who do not show a bilaminar cortex sign.

Bubble Signs

With the narrow mD dSIR sequence nulling white matter, bubble signs are seen with an increase in T_1 in white matter that crosses the high signal boundary ("overshoots") and enters the hD (Figure 16B) [5]. There is an outer high signal margin and a lower signal central region [3]. Bubble signs may also be seen in the gray matter of the thalamus and basal ganglia with narrow mD dSIR sequences when the T_1 in the gray matter decreases and crosses the bipolar T_1-filter peak. Bubble signs of this type may become more obvious with age, and are seen in Parkinson's disease. The decrease in T_1 in gray matter sufficient to cross the high signal boundary of narrow mD dSIR sequences is illustrated in Figure 20 and probably reflects heterogeneous distribution of free iron. Bubble signs may also be produced in MS by release of free iron at the rim of lesions decreasing the T_1 in abnormally increased T_1 lesions.

Figure 25 illustrates the origin of the bubble sign in the thalamus. The T_1 of lateral gray matter is decreased from normal ($TG_{latnorm}$) to abnormal (TG_{latab}). In doing so, it passes through the peak signal where there is a partial volume effect between $TG_{latnorm}$ and TG_{latab}. This results in a high signal on the periphery and a lower signal centrally in the bubble as shown by the vertical blue arrows in Figure 25.

 doi:10.20944/preprints202505.2380.v6

Primary Cerebral Hemisphere Cortices

The primary motor, somato-sensory and visual cortices layers IV-VI have relatively greater myelin than elsewhere in the cortex, and this results in a shorter T_1 and so the deep cortical signal is lower than the superficial signal from layers I-III when using narrow mD dSIR sequences compared with cortex elsewhere.

Clinical Use of T_2-FLAIR and Tissue Property-BLAIR (TP-BLAIR) Sequences

T_2-FLAIR and T_1-BLAIR sequences are complementary. The T_2-FLAIR images show contrast due to larger changes in T_2 and T_1-BLAIR sequences such as dSIR show abnormalities due to smaller changes in T_1 in white and/or gray matter in areas that appear normal or near normal with conventional T_2-FLAIR sequences (e.g., Figs. 16A and 16B). In many diseases there are concurrent increases in both T_1 and T_2 so that the T_1-BLAIR sequence can usefully be matched with a T_2-FLAIR sequence.

Other TP-BLAIR sequences can be used besides directly acquired dSIR sequences. These include synthetic dSIRs as well as T_2 and other tissue property synthetic TP- bipolar filters. Directly acquired TP-BLAIR sequences may be made sensitive to T_2, T_2* and D* as well as T_1 as composite bipolar filters e.g. T_1,T_2-BLAIR.

Other Sequences

The Double Inversion Recovery (DIR) Sequence

The DIR sequence multiples two IR sequences together and is one of the multiplied added subtracted and/or divided IR (MASDIR) group of sequences [5]. It has a doubly negative bipolar T_1-filter with two negative poles (Figure 26) [31] as well as ρ_m and T_2-filters. Initially, the two IR sequences were used to null fat and CSF [32] but in later versions of the sequence either white or gray matter was nulled and so was CSF [33]. Lesions which increase both T_1 and T_2 typically produce synergistic contrast. T_2 preparation can be used to produce synergistic T_2 contrast with that generated by the FSE data acquisition. This is synergistic with the T_1 contrast of the DIR sequence [34]. Incidental and/or intentional MT can also be used with the DIR sequence to increase lesion apparent ρ_m and T_1 contrast. The log DIR (lDIR) sequence can also be used to increase lesion contrast. White matter nulled DIR sequences can be of particular value for imaging lesions in the cerebral cortex.

In a study using a gray matter and CSF nulled DIR sequence in patients with MS so that only white matter signal remained, Tillema et al found a dark rim around lesions in white matter with longer T_1s [35]. The rim was due to nulling of T_1s in the boundary region between normal white matter and lesions. It was evident if the T_1 of the MS lesions was increased beyond the T_1 of nulled gray matter. This was seen more often in MS than other disease. The nulling effect is dependent on the T_1 of the mixture of tissues matching the first nulling TI of the DIR sequence. It corresponds to the high signal bubble sign seen in white matter (Figure 16B). Release of paramagnetic free iron could also have a role but the sign is due to T_1 effects, not susceptibility as with the paramagnetic rim sign seen with T_2*-weighted images.

Subtracted Inversion Recovery (SIR)

Enhanced viability imaging (ENVI) is a SIR sequence which is used for increased sensitivity in the detection of Gadolinium Based Contrast Agent (GBCA) induced T_1 shortening in cardiac studies [36].

Magnetisation Prepared 2 Rapid Acquisition Gradient Echo (MP2RAGE) [37-39]

This sequence multiplies the signals of two IR sequences together and divides this by the sum of the squares of the signals from the two sequences. Complex multiplication is employed. Signal values vary between ± ½. It is a negative unipolar T_1-filter for brain and has a moderate negative slope between white matter and gray matter with a shallower positive slope between gray matter

 doi:10.20944/preprints202505.2380.v6

and CSF (Figure 27, blue curve labelled FLAWS-uni which is identical with MP2RAGE). The sequence places white matter at the upper end of the display scale, gray matter at the lower end of the display scale and CSF at an intermediate level which is similar to the divided reverse SIR (drSIR) sequence but the reverse of the dSIR sequence.

The MP2RAGE sequence can be used to display dark rims around MS lesions [40]. The rims can be correlated with disease activity and are more predictive of this than paramagnetic rim signs. Similar to MP-RAGE, they reflect increases in T_1 that cross the lowest signal of the MP2RAGE negative unipolar T_1-filter shown in Figure 27 (blue curve). This work follows earlier studies in MS with a 3D IR gradient echo sequence [41] as well as the DIR study discussed earlier [35]. The signals in these cases are from the negative poles of IR sequences and correspond with the high signal seen with dSIR sequences at the outer boundary of MS lesions using the positive pole of the dSIR sequence (Figure 16B). Two of the five high signal lesions in Figure 16B show paramagnetic rim signs in Figure 16C. In comparison with the dark rims of the MP2RAGE and 3D IR gradient echo sequence, the dSIR sequence shows a more sharply defined boundary in keeping with the shape of its T_1-filter. The cut off points for showing dark rims or high signal boundaries can be changed by varying the relevant TI. There are also high signal rims seen at the margins of MS lesions which may be due to shortening of T_1 in normal white matter and/or lesions by paramagnetic "free" iron (as in Figure 6 of [41]). This may be made more obvious with a drSIR sequence sensitive to decreased T_1 with the longer TI nulling white matter [3].

Fluid and White Matter Suppression high contrast (FLAWS-hc), FLAWS- high contrast opposite (FLAWS-hco) and FLAWS-minimum (FLAWS-min) [42-45]

The FLAWS-hc and FLAWS-hco sequences have the same general mathematical form as the dSIR and drSIR sequences i.e. subtraction of two IR sequences divided by their sum i.e. $\frac{\text{difference}}{\text{sum}}$, but differ in important ways: firstly, the TIs used are widely separated as opposed to dSIR and drSIR sequences where the TIs are usually narrowly separated in order to specifically target small differences or changes in T_1 in tissues. Secondly, complex multiplication is used and the images are in phase-sensitive form not magnitude form. In Figure 27, the FLAWS-hc filter (green) has a positive slope over a very wide T_1 Domain and the FLAWS-hco filter (orange) has a negative slope over the same very wide Domain. The magnitude of the slopes of the two filters are generally greater than that of the FLAWS-min/MP2RAGE filter. The monotonic form of the FLAWS-hc and FLAWS-hco T_1-filters is strikingly different from the bipolar form of dSIR and lSIR T_1-filters which have well defined, sharp discontinuities at their null points due to the use of magnitude reconstruction. They also have steep positive slopes within narrow mDs rather than the broad lower magnitude slopes of the FLAWS-hc and FLAWS-hco filters over wide T_1 Domains (Figure 27).

The FLAWS-min filter is the lower signal from two IR T_1-filters, one nulling white matter and the other nulling CSF. This is typically divided by the sum of the signals from the two filters and has a maximum value of a ½ and a minimum value of zero for the brain. It follows the shorter TI nulling IR filter in the lower part and the longer TI nulling IR filter in the higher part of the T_1 Domain. It is a positive unipolar filter for the brain with the lowest signal nulling white matter, a peak at a T_1 just greater than the T_1 of gray matter, and CSF zero signal (Figure 27). It has similarities to the narrow mD dSIR sequence but has a lower display range and a lower slope. Müller et al described a halo sign when imaging MS lesions in the cortex with the FLAWS-min sequence (Figure 5 in reference [46]). This is due to an increase in cortex T_1 in lesions passing through the peak of the FLAWS-min filter into longer T_1 regions. The slope of the T_1-filter of the FLAWS-min sequence around its maximum value is relatively low and this may account for the greater width of the halo sign compared with the width of the bubble sign found with the narrow mD dSIR sequence when there is an increase in T_1 through the peak of that sequence (e.g. Figure 16B). There are also high signal boundaries between ventricular white matter and CSF as well as between white matter and a periventricular lesion with the FLAWS-min sequence (in Figure 5, reference [46]) as expected from its T_1-filter.

A similar pattern is seen in the leukocortical lesion shown in Figure 2B of reference [47] using T_1w-FLAWS which is the same as FLAWS-min. However, the cortical lesion shown in the same figure

 doi:10.20944/preprints202505.2380.v6

imaged with T_1w-FLAWS shows low contrast with the surrounding normal gray matter. Increased signal is seen at the boundary between gray matter and CSF. These features are consistent with Figure 27 (blue curve for FLAWS-min). FLAWS-min images do not show high signal between white matter and gray matter because the peak signal on the FLAWS-min T_1-filter is not between these two tissues. If the second nulling TI (of CSF) is reduced, the FLAWS-min sequence becomes more like a narrow mD dSIR filter but with lower magnitude slopes.

In summary, the MP2RAGE and FLAWS T_1-filters are unipolar or monotonic, not bipolar. They have fixed TIs and wide T_1 Domains with lower slopes than narrow mD dSIR bipolar T_1-filters in their mDs. The FLAWS-uni/MP2RAGE T_1-filter has a moderate slope, reduced CSF signal and shows white and gray matter at the upper and lower ends of the display scale. FLAWS-hc has a higher slope than FLAWS-uni/MP2RAGE, with CSF very high signal and a wide display range from WM to CSF. FLAWS-hco also has a higher magnitude negative slope than FLAWS-uni/MP2RAGE with CSF very low signal and a wide display range from CSF to white matter. FLAWS-min has a positive unipolar T_1-filter with a moderate slope and peak signal at a T_1 just greater than that of gray matter. The T_1-filters shown in Figure 27 provide a succinct and accessible way of comparing the signal levels and contrast performance of these sequences.

White Matter Nulled MP-RAGE [48] and Fast Gray Matter IR (FGATIR) [49]

These are single IR sequences that null white matter so that most of the remaining signal present in the brain is from gray matter. They have negative unipolar T_1-filters. The slopes of their T_1-filters are shown in Figure 6B and 6C when TI is chosen to null white matter. Small differences or changes in white matter from normal show much less contrast with white matter nulled MP-RAGE than with white matter nulled narrow mD dSIR sequences (Figure 6C). Boundaries between white matter and gray matter also show higher contrast with narrow mD sequences (Figure 7).

Tissue Border Enhancement [50], 3D-Edge Enhancing Gradient Echo (3D-EDGE) [51] and EDGE-MP2RAGE [52] Sequences

Tissue border enhancement (TBE) nulls signals at the junction between white and gray matter using spin echo acquisitions and was initially performed at 7T. It has a negative unipolar filter. The EDGE sequence has a single IR gradient echo and also uses a negative unipolar filter with a TI also chosen to produce zero signal at the boundary between white and gray matter with equal signals in each tissue using magnitude reconstruction. The low signal boundary seen with both techniques contains voxels with a mixture of the two tissues and a T_1 between those of white and gray matter. The techniques are of value in localising boundaries and diagnosing focal cortical dysplasia. EDGE-MP2RAGE acquires two separate images, the first of which is nulled in the same way as for the 3D-EDGE sequence. FGATIR, 3D-EDGE and EDGE-MP2RAGE images can be synthetically created from MP2RAGE derived T_1 maps [53].

 doi:10.20944/preprints202505.2380.v6

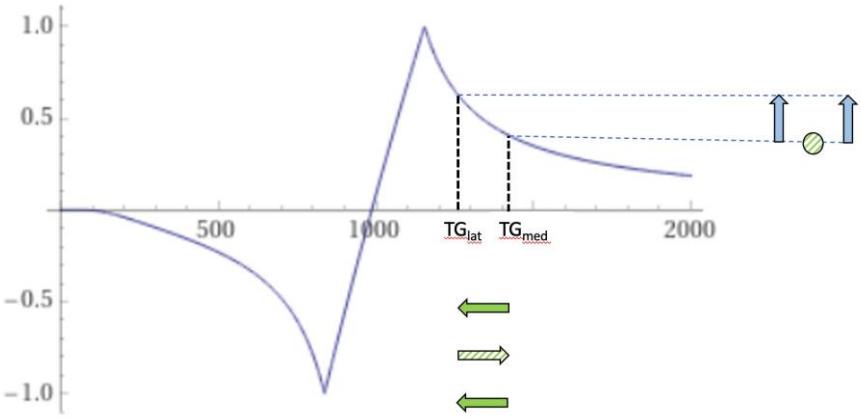

Figure 24. Thalamus. dSIR narrow mD (TI_s = 350 ms and TI_i = 500 ms) bipolar T_1-filter for normal appearance, abnormal increase in T_1 in lateral thalamic gray matter within the hD with loss of contrast with medial thalamic gray matter (striped green arrow) and subsequent decrease in T_1 to normal with restoration of contrast with medial thalamic gray matter (solid green arrow). The normal thalamus gray matter shows a decrease in T_1 from medial (TG_{med}) to lateral (TG_{lat}) (highest horizontal negative solid green arrow) and corresponding positive contrast (first vertical positive blue arrow). With disease, there is an increase in T_1 in the lateral thalamus (middle horizontal positive striped green arrow) with a loss of contrast with the medial thalamus (blue circle). With later regression of this and return of the T_1 difference between the lateral and medial thalamus to normal (lowest negative solid green arrow), normal positive contrast is seen between the medial and lateral thalamus (second vertical positive blue arrow).

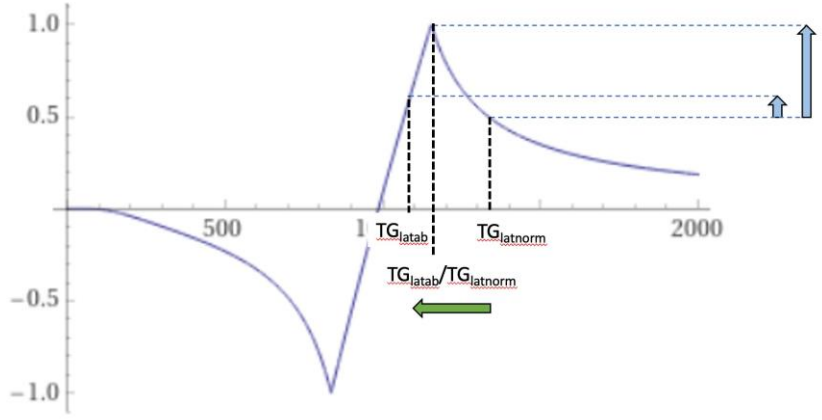

Figure 25. Thalamus. Narrow mD (TI_s = 350 ms and TI_i = 500 ms). dSIR bipolar T_1-filter for a larger abnormal decrease in T_1 in lateral thalamic gray matter from normal ($TG_{latnorm}$) to abnormal (TG_{latab}) extending from the hD through the signal peak to the mD (horizontal negative green arrow). Signal in the lateral thalamus is highest where there is partial volume effect between abnormal and normal gray matter of the thalamus ($TG_{latab}/TG_{latnorm}$) (longer vertical blue arrow). Signal from abnormal lateral thalamus in the middle Domain (TG_{latab}) (shorter blue arrow) is less than the signal in the lateral thalamus at the boundary between normal and abnormal thalamus (longer blue arrow). The higher and lower signals (vertical blue arrows) result in a bubble sign with higher signal in the periphery where there are partial volume effects and lower signal centrally where there is only abnormal gray matter. The same argument applies to the medial thalamus.

 doi:10.20944/preprints202505.2380.v6

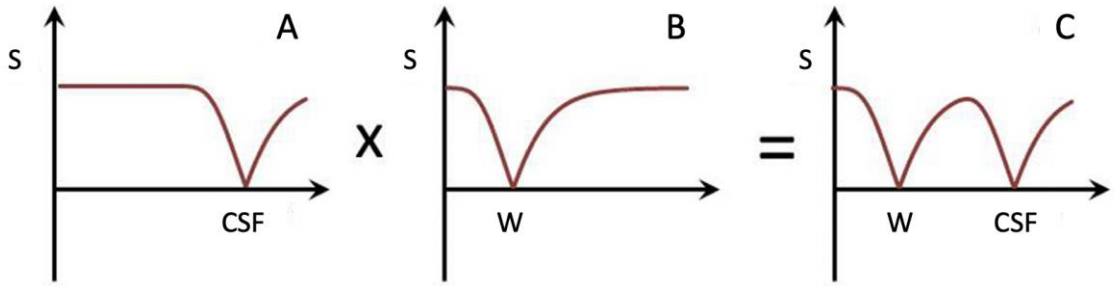

Fig. 26. A DIR sequence bipolar T_1-filter for imaging the brain. (A) is the IR T_1-filter nulling CSF, (B) is the IR T_1-filter nulling white matter (W), and (C) is (A) multiplied by (B) in which both W and CSF are nulled. (C) is the DIR bipolar T_1-filter. It has two negative poles.

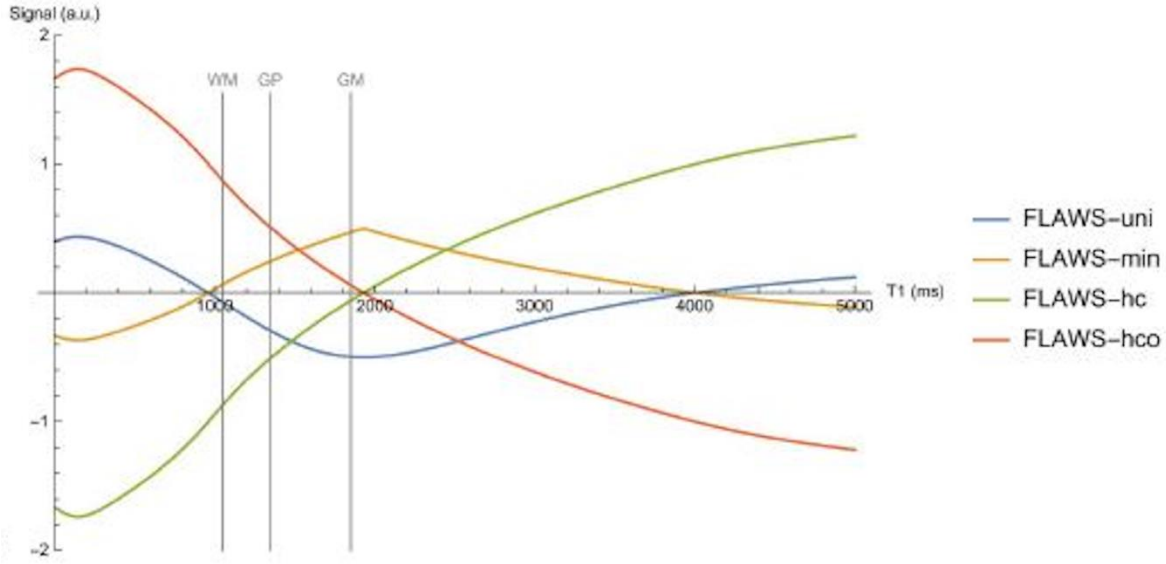

Figure 27. Plots of signal vs T_1 (T_1-filters) for the FLAWS-uni/MP2RAGE (blue), FLAWS-min (yellow), FLAWS-hc (green) and FLAWS-hco (orange) T_1-filters from Beaumont et al Fig 1B in reference [24].The FLAWS-uni/MP2RAGE T_1-filter (blue) is a negative unipolar T_1-filter for brain and CSF with a moderate negative slope between white matter (WM) and gray matter (GM), and a moderate positive slope between GM and CSF at 4000 ms. The CSF and WM signals are similar. The display range is from GM to WM. (GP is the globus pallidus).The FLAWS-min T_1-filter (yellow) is a positive unipolar T_1-filter with a moderate positive slope from WM to beyond GM and a moderate negative slope from this point to CSF with CSF low signal. The display range is from WM and CSF to just higher than GM.The FLAWS-hc T_1-filter (green) is monotonic for brain and CSF. It has a higher positive slope than the magnitude of the FLAWS-min/MP2RAGE slope from WM to GM and CSF has a very high signal. WM is at the lowest level on the display range and CSF is at the highest level. The FLAWS-hco T_1-filter is monotonic with a higher size of slope than FLAWS-uni/MP2RAGE between WM and GM and a very low signal for CSF. The display range is from CSF to white matter.*(Reproduced with permission: from Beaumont et al [24])*

Conclusions

BLAIR sequences provide increased lesion contrast and better defined tissue boundaries using T_1, T_2, MT and other tissue properties and can be readily implemented using existing sequences on MR systems. BLAIR sequences are sensitive to small changes in T_1, T_2 and other tissue properties and

 doi:10.20944/preprints202505.2380.v6

are complementary to conventional sequences such as T_2-FLAIR which are sensitive to larger changes in tissue properties.

A limitation of this paper is that it is educational in content and designed to facilitate implementation of the new sequences and interpretation of the resultant images rather than to provide an account of detailed studies using the new sequences. This is because the educational aspect is seen as a necessary prelude to systematic clinical studies which will be required to establish the efficacy of BLAIR sequences

Funding: We have received support from the Fred Lewis Enterprise Foundation, the Hugh Green Foundation, Manaaki Moves, NZ P Pull, the JN & HB Williams Foundation, the Mangatawa Beale Williams Memorial Trust, Neurological Foundation, Trust Tairāwhiti, Friends of Mātai Blue Sky Fund, GE Healthcare, Mātai Ngā Māngai Maori, and Kānoa— Regional Economic Development & Investment Unit of New Zealand.

Statement and Declarations: Conflict of interest: GMB is a consultant to Magnetica, Brisbane, Australia. No other authors have any conflict of interest to disclose.

Ethical approval: All procedures performed in the studies involving human participants were in accordance with the ethical standards of the institutional and/or national research committee and with the 1964 Helsinki Declaration and its later amendments or comparable ethical standards.

Informed consent: Written informed consent was obtained from all participants in this study.

Key Points

- Ultra-high contrast MRI using BipoLAr Inversion Recovery (BLAIR) images can show abnormalities with very high contrast where little or no change from normal is seen with common conventional state-of-the-art images.
- The abnormalities shown with ultra-high contrast are due to small changes in tissue properties such as T_1 and T_2 in disease. This is complementary to existing sequences which show abnormalities due to larger changes in T_1 and T_2 in disease.
- At boundaries between tissues and fluids on ultra-high contrast images there is frequently an increase in contrast and an increase in the spatial resolution of that contrast.
- Extensive abnormalities were seen in mild traumatic brain injury, multiple sclerosis and white matter associated with cerebral tumours on BLAIR images in the absence of changes in T_2-weighted spin echo or T_2-FLAIR images.
- Four types of BLAIR sequences are described. Implementation of these does not require any increase in static or gradient magnetic field. They can be easily implemented on existing MR systems at very little cost.

 doi:10.20944/preprints202505.2380.v6

Abbreviations

BLAIR	BipoLAr Inversion Recovery
cdSIR	composite divided Subtracted Inversion Recovery
clSIR	composite logarithmic then Subtracted Inversion Recovery
DIR	Double Inversion Recovery
dSIR	divided Subtracted Inversion Recovery
ENVI	ENhanced Viability Imaging
hD	highest Domain
IR	Inversion Recovery
lD	lowest Domain
lSIR	logarithmic then Subtracted Inversion Recovery
mD	middle Domain
MP2RAGE	Magnetisation Prepared 2 Rapid Acquisition Gradient Echo
MT	Magnetisation Transfer
RE	Reactive Encephalopathy
SIR	Subtracted Inversion Recovery
S_{OF}	Signal from Other Filter
TP	Tissue Property
TP-filter	Tissue Property-filter
UHC	Ultra-High Contrast

 doi:10.20944/preprints202505.2380.v6

References

1. Condron P, Cornfeld DM, Scadeng M, et al (2024) Ultra-high contrast MRI: the whiteout sign shown with divided subtracted inversion recovery (dSIR) sequences in post-insult leukoencephalopathy syndromes (PILS). Tomography 10(7):983-1013
2. Ma Y-J, Shao H, Fan S, et al (2020) New options for increasing the sensitivity, specificity and scope of synergistic contrast magnetic resonance imaging (scMRI) using Multiplied, Added, Subtracted and/or FiTted (MASTIR) pulse sequences. Quant Imaging Med Surg 10(10):2030-2065
3. Ma Y-J, Moazamian D, Port JD, et al (2023) Targeted magnetic resonance imaging (tMRI) of small changes in the T_1 and spatial properties of normal and near normal appearing white and gray matter in disease of the brain using divided subtracted inversion recovery (dSIR) and divided reverse subtracted inversion recovery (drSIR) sequences. Quant Imaging Med Surg 13(10):7304-7337
4. Newburn G, McGeown JP, Kwon EE, et al (2023) Targeted MRI (tMRI) of small increases in the T_1 of normal appearing white matter in mild traumatic brain injury (mTBI) using a divided subtracted inversion recovery (dSIR) sequence. OBM Neurobiology 7(4): doi: 10.21926/obm.neurobiol.2304201
5. Ma Y-J, Moazamian D, Cornfeld DM, et al (2022) Improving the understanding and performance of clinical MRI using tissue property filters and the central contrast theorem, MASDIR pulse sequences and synergistic contrast MRI. Quant Imaging Med Surg 12(9):4658-4690
6. Cornfeld D, Condron P, Newburn G, et al (2024) Ultra-high contrast MRI: Using divided subtracted inversion recovery (dSIR) and divided echo subtraction (dES)sequences to study the brain and musculoskeletal system. Bioengineering 11:441
7. Newburn G, Condron P, Kwon EE, et al (2024) Diagnosis of delayed post-hypoxic leukoencephalopathy (Grinker's myelinopathy) with MRI using divided subtracted inversion recovery (dSIR) sequences: time for reappraisal of the syndrome? Diagnostics 14(4):418. https://doi.org/10.3390/diagnostics14040418
8. Yokoo T, Bae WC, Hamilton G, et al (2010) A quantitative approach to sequence and image weighting. J Comput Assist Tomogr 34(3):317-331
9. Young IR, Szeverenyi NM, Du J, Bydder GM (2020) Pulse sequences as tissue property filters (TP-filters): a way of understanding the signal, contrast and weighting of magnetic resonance images. Quant Imaging Med Surg 10(5):1080-1120
10. Bydder, M., Cornfeld, D.M., Melzer, T.R. et al (2025) Log subtracted inversion recovery. Magn Reson Imaging 117:110328
11. Ugurbil K (2014) Magnetic resonance imaging at ultrahigh fields. IEE Trans Biomed Eng 61:1364-1379
12. Platt R, Ladd ME, Paech D (2021) 7 Tesla and Beyond: Advanced methods and clinical applications in magnetic resonance imaging. Invest Radiol 56(11):705-725
13. Ivanov D, De Martino F, Formisano E, et al (2023) Magnetic resonance imaging at 9.4 T: the Maastricht journey. MAGMA 36(2):159-173
14. Ladd ME, Quick HH, Speck O, et al (2023) Germany's journey towards 14 Tesla human magnetic resonance. MAGMA 36(2):191-201
15. Bates S, Dumoulin SO, Folkers PJM et al (2023) A vision of 14 T MR for fundamental and clinical science. MAGMA 36(2):211-225
16. Vachha B, Huang SY (2021 MRI with ultrahigh field strength and high-performance gradients: challenges and opportunities for clinical neuroimaging at 7 T and beyond. Eur Radiol Exp 5(1):35
17. Feinberg DA, Beckett AJS, Vu AT, et al (2023) Next-generation MRI scanner designed for ultra-high-resolution human brain imaging at 7 Tesla. Nat Methods 20:2048-2057
18. Bydder M, Condron P, Cornfeld DM, et al (2024) Validation of an ultra-high contrast divided subtracted inversion recovery technique using a standard T_1 phantom. NMR Biomed 2024;e5269
19. Losa L, Peruzzo D, Galbiati S, Locatelli F, Agarwal N (2024) Enhancing T_1 signal of normal-appearing white matter with divided subtracted inversion recovery: a pilot study in mild traumatic brain injury. NMR Biomed 37(10):e5175
20. Kauppinen RA, Thotland J, Pisharady PK, Lenglet C, Garwood M (2025) A subtracted-added-divided inversion recovery (dSIR) approach to visualise the effects of microstructure on T_1 contrast in human white matter. NMR Biomed 38(7):e70070

 doi:10.20944/preprints202505.2380.v6

21. Hajnal JV, Baudouin CJ, Oatridge A, Young IR, Bydder GM (1992) Design and implementation of magnetisation transfer pulse sequences for clinical use. J Comput Assist Tomogr 16(1):7-18
22. Dortch RD, Bagnato F, Gochberg DF, Gore JC, Smith SA (2018) Optimization of selective inversion recovery magnetization transfer imaging for macromolecular content mapping in the human brain. Magn Reson Med 80(5):1824-1835
23. Cronin MJ, Xu J, Bagnato F, Gochberg DF, Gore JC, Dortch RD (2020) Rapid whote-brain quantitative magnetization transfer imaging using 3D selective inversion recovery sequences. Magn Reson Imaging 68:66-74
24. Demir S, Clifford B, Lo W-C, et al (2022) Optimization of magnetization transfer contrast for EPI FLAIR brain imaging. Magn Reson Med 87(5):2380-2387
25. Bagnato F, Franco G, Ye F, et al (2020) Selective inversion recovery quantitative magnetization transfer imaging: Toward a 3T clinical application in multiple sclerosis. Mult Scler 26(4):457-467
26. Kusama M, Kimur Y, Yoneyama M et al (2025) Comparison of 3D magnetization transfer and spectral presaturation with inversion recovery based Neuromelanin Imaging. Magn Reson Med Sci 24:184-190
27. Toubasi AA, Lakhani DA, Cutter G, et al (2025) Improving the detection of myelin integrity in multiple sclerosis using selective inversion recovery for MRI with quantitative magnetization transfer. J Magn Reson Imaging 61(6):2444-2454
28. Nürnberger L, Gracien R-M, Hok P, et al (2017) Longitudinal changes of cortical microstructure in Parkinson's disease assessed with T_1 relaxometry. NeuroImage Clinical 13:405-414
29. Roeben B, Zeltner L, Hagberg GE, Scheffler K, Schols L, Bender B (2023) Susceptibility-weighted imaging reveals subcortical iron deposition in PLA2G6-associated neurodegeneration: the "Double Cortex Sign". Mov Disord 38(5):904-906
30. Mueller SG (2024) 7T MP2RAGE for cortical myelin segmentation: impact of aging. PLoS One 19(4):e0299670
31. Ma Y-J, Fan S, Shao H, et al (2020) Use of multiplied, added, subtracted and/or fitted inversion recovery (MASTIR) pulse sequences. Quant Imaging Med Surg 10(6):1334-1369
32. Bydder GM, Young IR (1985) MR imaging: clinical use of the inversion recovery sequence. J Comput Assist Tomogr 9(4):659-675
33. Redpath TW, Smith FW (1994) Technical note: use of a double inversion recovery pulse sequence to image selectively grey or white brain matter. Br J Radiol 67(804):1258-1263
34. Costagli M, Lapucci C, Zacà D, et al (2022) Improved detection of multiple sclerosis lesions with T_2-prepared double inversion recovery at 3T. J Neuroimaging 32:902- 909
35. Tillema J-M, Weigand SD, Dayan M, et al (2018) Dark rims: novel sequence enhances diagnostic specificity in multiple sclerosis. AJNR Am J Neuroradiol 39(6):1052-1058
36. Foo TKF, Wolff SD, Gupta SN, Kraitchman DL (2005) Enhanced viability imaging: Improved contrast in myocardial delayed enhancement using dual inversion time subtraction. Magn Reson Med 53:1484-1489
37. Marques JP, Kober T, Krueger G, van der Zwaag W, Van de Moortele P-F, Gruetter R (2010) MP2RAGE, a self bias-field corrected sequence for improved segmentation and T_1-mapping at high field. Neuroimage 49(2):1271-1281
38. Kober T, Granziera C, Ribes D, et al (2012) MP2RAGE multiple sclerosis magnetic resonance imaging at 3 T. Invest Radiol 47(6):346-352
39. Aichour R, Emorine T, Oubaya N, et al (2025) Improved MR detection of optic nerve demyelination with MP2RAGE-FLAWS compared with T_2-weighted fat saturated sequences. Invest Radiol 60(6):387-396
40. Marshall M, Aphiwatthanasumet K, Mougin O, et al (2025) T_1-dark-rim as a marker of new and chronic active multiple sclerosis lesions: A serial study with frequent 7T MRI. J Neuroimaging 35(3):e70044
41. Naval-Baudin P, Pons_escoda A, Castillo-Pinar A, et al (2024) The T_1-dark-rim: A novel imaging sign for detecting smoldering inflammation in multiple sclerosis. Eur J Radiol 173:111358
42. Beaumont J, Saint-Jalmes H, Acosta O, et al (2019) Multi T_1-weighted contrast MRI with fluid and white matter suppression at 1.5T. Magn Reson Imaging 63:217-225
43. Beaumont J, Gambarota G, Saint-Jalmes H, et al (2021) High-resolution multi-T_1-weighted contrast and T_1 mapping with low B_1 sensitivity using the fluid and white matter suppression (FLAWS) sequence at 7T. Magn Reson Med 85(3):1364-1378
44. Muller J, Rahmanzadeh R, Tsgkas C, et al (2021) Cortical lesion detection using FLAWS in multiple sclerosis. Mult Scler 27(2):433-434

 doi:10.20944/preprints202505.2380.v6

45. Beaumont J, Fripp J, Raniga P, et al (2023) Multi T_1-weighted contrast imaging and T_1 mapping with compressed sensing FLAWS at 3 T. MAGMA 36(5):823-836
46. Müller J, La Rosa F, Beaumont J, et al (2022) Fluid and white matter suppression. New sensitive 3T magnetic resonance imaging contrasts for cortical lesion detection in multiple sclerosis. Invest Radiol 57(9):592-600
47. Durozard P, Maarouf A, Zaaraoui W, et al (2024) Cortical lesions as an early hallmark of Multiple Sclerosis: visualization by 7T MRI. Invest Radiol 59(11):747- 753
48. Saranathan M, Tourdias T, Bayram E, Ghanouni P, Rutt BK (2015) Optimization of white-matter-nulled magnetization prepared rapid gradient echo (MP-RAGE) imaging. Magn Reson Med 73(5):1786-1794
49. Grewal SS, Middlebrooks EH, Kaufmann TJ, et al (2018) Fast gray matter acquisition T_1 inversion recovery MRI to delineate the mammillothalamic tract for preoperative direct targeting of the anterior nucleus of the thalamus for deep brain stimulation in epilepsy. Neurosurg Focus 45(2):E6. doi:10.3171/2018.4.FOCuS18147
50. Costagli M, Kelley DAC, Symms MR et al (2014) Tissue border enhancement by inversion recovery MRI at 7T. Neuroradiology 56:517-523
51. Middlebrooks EH, Lin C, Westerhold E, et al (2020) Improved detection of focal cortical dysplasia using a novel 3D imaging sequence: Edge-Enhancing Gradient Echo (3D-EDGE) MRI. NeuroImage 28:102449
52. Tao S, Zhou E, Greco V, et al (2023) Edge-Enhancing Gradient-Echo MP2RAGE for clinical epilepsy imaging at 7T. AJNR Am J Neuroradiol 44(3):268-270
53. Middlebrooks EH, Tao S, Zhou X, et al (2023) Synthetic inversion image generation using MP2RAGE T_1 mapping for surgical targeting in deep brain stimulation and lesioning. Stereotact Funct Neurosurg 101:326-331